ORIGINAL ARTICLE

A rationally designed CD19 monoclonal antibody-triptolide conjugate for the treatment of systemic lupus erythematosus

Lai Wang[a,b,†], Haoyuan Yin[a,b,†], Jiao Jiang[a,b,†], Qilin Li[b,d],
Changxing Gao[a,b], Wenrui Li[a,b], Bo Zhang[a,b], Yue Xin[a,b],
Hongyang Li[a,c], Ming Zhao[a,b,*], Qianjin Lu[a,b,*]

[a]*Hospital for Skin Diseases, Institute of Dermatology, Chinese Academy of Medical Sciences and Peking Union Medical College, Nanjing 210042, China*
[b]*Key Laboratory of Basic and Translational Research on Immune-Mediated Skin Diseases, Chinese Academy of Medical Sciences, Nanjing 210042, China*
[c]*Jiangsu Key Laboratory of Molecular Biology for Skin Diseases and STIs, Nanjing 210042, China*
[d]*Hunan Key Laboratory of Medical Epigenomics, the Second Xiangya Hospital, Central South University, Changsha 410011, China*

Abstract *Tripterygium wilfordii* Hook F (TWHF) is a traditional Chinese medicine widely used in the treatment of systemic lupus erythematosus (SLE), with triptolide (TP) as its main active ingredient. However, its side effects also induced by TP, especially hepatotoxicity and reproductive toxicity, largely limit its application in a subset of patients. Monoclonal antibodies (mAbs) developed for the treatment of SLE that deplete B cells by targeting B cell-expressing antigens, such as CD19, have failed in clinical trials, partly due to their poor efficacy in consuming B cells. Here, we report the development of a rationally designed antibody−drug conjugate (ADC), CD19 mAb-TP conjugate, to alleviate the side effects of TWHF and simultaneously improve the therapeutic efficacy of CD19 mAb. The CD19 mAb-TP conjugate, which was named ADC-TP, selectively depleted B cell subsets both *in vitro* and *in vivo* and effectively alleviated disease symptoms in mouse lupus models with enhanced therapeutic efficacy than CD19 mAb and fewer side effects than TP. Our present study proposes a CD19 mAb−TP conjugate strategy to mitigate the toxicity of TWHF while also enhancing the therapeutical efficacy of CD19 mAbs for the treatment of SLE, providing a feasible method for improving the current agents used for treating SLE.

---

*Corresponding authors.
   E-mail addresses: zhaoming301@pumcderm.cams.cn (Ming Zhao), qianlu5860@pumcderm.cams.cn (Qianjin Lu).
   †These authors made equal contributions to this work.

1. Introduction

Tripterygium wilfordii Hook F (TWHF) is a widely used traditional Chinese medicinal plant whose extracts have been used as anti-inflammatory and immunosuppressive remedies for centuries[1]. More than 300 compounds have been identified from extracts of TWHF. Of these, many are diterpenoids, three of which dominate the chemical profile and the medicinal chemistry of TWHF, including triptolide (TP), tripdiolide, and triptonide[2]. TWHF exerts its anti-inflammatory and immunoregulatory activities mainly in two ways. On the one hand, the major diterpenoids of TWHF can suppress cytokine transcription and other proinflammatory genes by inhibiting related inflammatory signaling pathways, such as ERK1/2-NF-κB and JAK/STAT signaling pathways[3,4]. On the other hand, the major diterpenoids of TWHF can regulate cell differentiation of immune cells or directly induce the death of immune cell death[5-7]. However, despite the impressive therapeutical effects on disease activity of autoimmune diseases and inflammatory disorders, side effects elicited by TWHF, including but not limited to hepatotoxicity, nephrotoxicity, and reproductive toxicity, are ineligible issues[8-10]. In addition, long-term administration of TWHF was reported to have decreased bone mineral density (BMD) levels in female patients with systemic lupus erythematosus (SLE), indicating that osteoporosis may be an essential problem for SLE patients treated with TWHF[11]. Unfortunately, the toxic ingredients of TWHF, especially TP, are just right in their medicinal composition, meaning that they cannot be eliminated in the clinical use of TWHF. Various delivery strategies have been designed to limit the adverse effects and enhance the efficacy of TP, but none have been successfully applied in clinical practice[12,13].

SLE is an autoimmune disease that affects multiple systems and organs and is more common in women of childbearing age aged 20−40[14]. It is estimated that the global prevalence of SLE is 43.7 per 100,000 people. Among women, the value is as high as 78.73 per 100,000 people[15]. The incidence rate is higher among Black, Asian, and Hispanic populations. SLE lesions involve the skin, skeletal system, respiratory system, cardiovascular system, etc. Renal failure and brain damage are common causes of death in SLE patients, with a mortality rate 2−3 times higher than the general population[16]. At present, the drugs used in clinical practice to treat SLE mainly include antimalarial drugs, glucocorticoids, immunosuppressants, and monoclonal antibodies[17]. Long-term use of the antimalarial drug hydroxychloroquine poses a risk of retinal and corneal lesions. Long-term and large-dose use of glucocorticoids can cause secondary complications such as infection, hypertension, diabetes, osteoporosis, etc. Immunosuppressants such as cyclophosphamide can effectively treat lupus nephritis. Still, there are potentially severe side effects, including bone marrow suppression, infection, liver and kidney function damage, and gonadal suppression[18]. However, the immunological events that trigger the onset of clinical manifestations have not yet been fully defined. The central role of B cells in the pathogenesis of SLE has more recently gained prominence[19]. Therefore, B cell-targeted therapy has become one of the most promising treatment strategies for SLE[20]. The treatment approaches to target the B cell compartment can be broadly summarized as direct depletion, typically with monoclonal antibodies (mAbs) (*e.g.*, rituximab targeting CD20), indirect depletion *via* survival cytokine blockade (*e.g.*, belimumab targeting BLyS) and co-stimulatory blockade[20]. However, belimumab is so far the only biological agent approved by the U.S. Food and Drug Administration (FDA) in 2011 for the treatment of SLE[21], and no biological agent that directly depletes B cells has been approved. Although CD20-targeted rituximab has achieved great success in the treatment of malignant hematological tumors, two trials of rituximab in patients with SLE and lupus nephritis failed to meet their respective primary endpoints[22-24]. Insufficient tissue B cell depletion in at least a subset of lupus patients could explain the failure of rituximab to reach clinical endpoints[25], which may be attributed to the compromised antibody-dependent cellular cytotoxicity (ADCC) in these patients[26]. Thus, newly developed CD20-targeted mAb with greater ability in B cell depletion was reported to be more efficacious in the amelioration of disease[27].

Additionally, targeting CD19 has emerged as a promising new approach for improving the treatment of autoimmune diseases. A humanized anti-human CD19 mAb, inebilizumab, has been evaluated in a model of autoimmunity involving mice transgenic (Tg) for *Sle1* and human CD19. Inebilizumab treatment resulted in a robust reduction of autoantibodies but had minimal effect on total serum immunoglobulins[28]. However, in the phase II clinical trial, obexelimab, a human anti-CD19 mAbs, did not meet the primary endpoint[29]. However, previous studies have shown that sustained B cell depletion by CD19-targeted chimeric antigen receptors (CARs) T cells effectively treat murine lupus[30,31]. CD19-targeted CAR T cell therapy has recently been tested in refractory SLE patients and has significantly alleviated disease activity[32,33]. These studies indicate that CD19 is a feasible therapeutical target for SLE, but CD19-targeted mAbs alone may be less effective in adequately eliminating B cells. Thus, increasing the capacity of B cell-targeting mAbs to deplete B cells could make them more efficacious in SLE treatment.

Antibody-drug conjugates (ADCs) are an emerging class of immuno-chemotherapeutics featuring the structure of a mAb conjugated to cytotoxic agents (warheads) *via* chemical linkers. Compared with chemical drugs, ADC drugs possess more excellent targeting capability, which may lead to less "off-target"-induced toxicity. Compared with mAb drugs, ADC drugs possess more potent cytotoxicity and can achieve more effective disease control. Despite the success of ADCs achieved in various types of cancer[34], no ADCs have been applied to treat SLE in clinics. In the present study, we rationally designed a CD19 mAb-TP conjugate and evaluated its efficacy for treating SLE *in vitro* and *in vivo* (Scheme 1). CD19 mAb-TP conjugate selectively depleted CD19$^+$ B cells in *in vitro* experiments and showed impressive therapeutic effects in *in vivo* murine lupus models. Notably, the efficacy of CD19 mAb-TP was superior to TP and CD19 mAb, and the adverse reactions were significantly milder than that of TP. The results presented here propose a rational-designed CD19 mAb-TP conjugate to mitigate the toxicity of TWHF while also
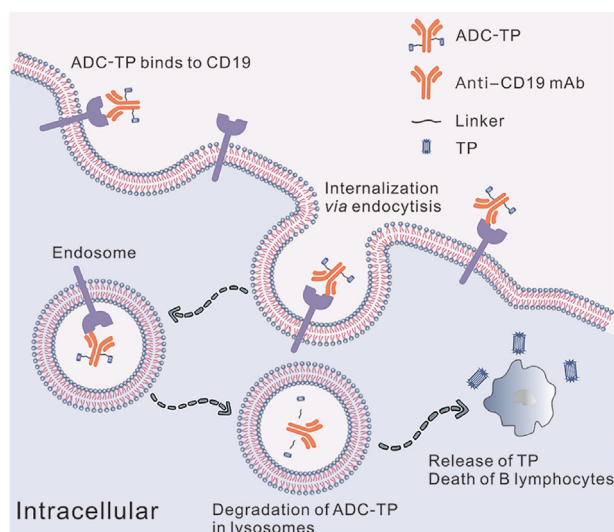
Scheme 1 The ADC targeting CD19 loaded with TP has been constructed for clinical treatment of SLE to alleviate toxicity of TP and enhance the efficacy of monoclonal antibodies.

enhancing the therapeutical efficacy of CD19 mAb for the treatment of SLE and provides a feasible strategy for improving current agents used to treat SLE.

2. Materials and methods

2.1. Materials

Anti-mouse CD19 mAb (clone #1D3, BE0150) and IgG2a (BE0089) isotype controls were purchased from Bioxcell (West Lebanon, NH, USA). Anti-human CD19 mAbs Denintuzumab (HY-P99285) and Inebilizumab (HY-P99113) were purchased from MedChemExpress (NJ, USA). Cyanine 7 (Cy7)-conjugated Triptolide (R-TPD-7) and TP-PEG$_{2000}$-NHS (R-NPL-1000) were obtained from Xi'an Ruixi Biological Technology Co., Ltd. (Xi'an, China). TP (38748-32-2) was obtained from Shanghai Yuanye Bio-Technology Co., Ltd. (Shanghai, China). AST activity assay kit (BC1565), ALT activity assay kit (BC-1555), and creatinine activity assay kit (BC1535) were purchased from Beijing Solarbio Science & Technology Co., Ltd. (Beijing, China). Mouse anti-double stranded DNA antibody (IgG) ELISA Kit (CSB-E11194m) and Mouse anti-nuclear Antibody (IgG) ELISA Kit (CSB-E12912m) were purchased from CUSABIO (Wuhan, China). Gibco Dulbecco's modified Eagle's medium (DMEM) (C11995500BT) and RPMI-1640 medium (C11875500BT) were purchased from Invitrogen (Karlsbad, CA, USA).

2.2. Mice and cell lines

Lupus-prone MRL/MpJ-*Fas^{lpr}* (MRL/*lpr*) mice and their control strain MRL/MpJ mice were purchased from the Shanghai Laboratory Animal Center of the Chinese Academy of Sciences (Shanghai, China). Female C57BL/6J mice and female ICR mice were purchased from the Laboratory Animal Center of Yangzhou University (Yangzhou, China). All experimental procedures were executed according to the protocols approved by the Review Committee of the Chinese Academy of Medical Science & Peking Union Medical College. All animal experiments comply with the

National Research Council's Guide for the care and use of laboratory animals (Approval number: 2022 Animal No. 016). Human normal liver HL-7702 cell line, Madin−Darby canine kidney (MDCK) cell line, human lymphoblastoid GM12878 cell line, mouse BAF3 pro-B cell lines, human Jurkat cell line, mouse A20 B cell lymphoma cell line and mouse EL4 T cell lymphoma cell line for *in vitro* studies were purchased from American Type Culture Collection (ATCC) (Mansas, VA, USA).

2.3. Construction of CD19 mAb-TP conjugates

TP-PEG$_{2000}$-NHS and CD19 mAb were dissolved in an appropriate amount of pure water and phosphate-buffered saline (PBS) (P1020, Solarbio), respectively. Then, TP-PEG$_{2000}$-NHS solution and CD19 mAb solution were mixed in a ratio of 10:1, and the mixed solution was slowly stirred for reactions at room temperature for 3 h. Excessive TP-PEG$_{2000}$-NHS (with a cut-off molecular weight of 10 kDa, dialysis medium was pure water) was removed by dialysis. CD19 mAb-TP conjugate was obtained.

2.4. Determination of DAR value

LC−MS/MS analysis was employed to determine the DAR value. Chemicals and instrumentation: formic acid (FA), acetonitrile (ACN), and methanol were purchased from Sigma−Aldrich (St. Louis, MO, USA). Ultrapure water was prepared from a Millipore purification system (Milli-Q SQ2, Billerica, MA, USA). An Ultimate 3000 coupled with an AB SCIEX TripleTOF 5600 Mass Spectrometer (AB SCIEX, Boston, MA, USA) with an ESI nanospray source. Sample preparation: Take an appropriate amount of protein solution into a 1.5 mL EP tube, centrifuge at 12,000 rcf (Centrifuge 5810 R, Eppendorf, Hamburg, Germany) for 10 min at 4 °C, and take the supernatant for standby. LC−MS/MS analysis was performed as follows. For UPLC: Ultimate 3000 (Thermo Fisher Scientific, Waltham, MA, USA). Column: ACQUITY UPLC Protein BEH C4 Column (300 Å, 1.7 μm, 2.1 mm × 50 mm); Mobile phase: A: 0.1% formic acid in water; B: 0.1% formic acid in acetonitrile. Total flow rate: 0.300 mL/min. LC linear gradient: from 5% to 100% B for 10 min, from 100% to 100% B for 3 min, from 100% to 5% B for 1 min, from 5% to 5% B for 1 min. For mass spectrometry: AB SCIEX TripleTOF 5600 Mass Spectrometer; Mass range: *m/z* 300−4000.

2.5. Internalization studies

The antibody internalization and lysosome co-localization of cells were qualitatively evaluated by immunofluorescence. In short, A20 and EL4 were incubated with ADC-TP at 37 °C for 0.5, 2, 4, and 6 h, respectively. After infiltrating cells with Tween-20 (0.1% phosphate buffer) from each time point, the samples were washed with PBS. Subsequently, rabbit LAMP-1 monoclonal antibody (MA5-29385, Invitrogen) was added, and the samples were incubated on ice for 1 h. After washing, the samples were added with anti-rat IgG Rhodamine antibody (AS022, ABclonal, Wuhan, China) or anti-rat IgG-AF488 antibody (A-11006, Invitrogen) to detect ADC-TP and anti-rabbit IgG-FITC (65-6111, Invitrogen) to detect Lysosome. Use DAPI dye (C1006, Beyotime, Shanghai, China) to stain the nucleus. Qualitative analysis was achieved through fluorescence microscopy (OLYMPUS-BX53, Olympus, Tokyo, Japan) examination.

2.6. Treatment of MRL/lpr mice

After one week of adaptive feeding, urine samples were collected from female MRL/lpr mice, and urinary protein (Upro) levels were assessed by a colorimetric assay strip (URIT1V, URIT, Guilin, China). The female MRL/lpr mice serum samples were collected, and serum anti-dsDNA IgG levels were detected using ELISA. Then, these female MRL/lpr mice aged 16 weeks were divided into five groups according to Upro levels and serum anti-dsDNA IgG levels, with MRL/MpJ mice as negative control ($n = 6$ per group). Mice in the TP group were intraperitoneally injected with 0.05 mg/kg TP thrice weekly. Mice in the TP-PEG group were intraperitoneally injected with 0.375 mg/kg TP-PEG thrice weekly, maintaining the same molar amount as TP. According to the average DAR value of ADC-TP (4.75), mice in the ADC-TP group were intraperitoneally injected with 4.4 mg/kg ADC-TP three times per week, maintaining the same molar amount as TP-PEG. Mice in the CD19 mAb group were intraperitoneally injected with 4.4 mg/kg CD19 mAb thrice weekly, keeping the same amount of CD19 mAb as ADC-TP. The serum samples of MRL/lpr mice and MRL/MpJ mice were collected at the beginning and end of the observation period. The serum anti-dsDNA IgG levels were detected by ELISA. Spleens and dLNs were used to execute immune cell analysis by flow cytometry (BD LSRFortessa, BD, Franklin Lake, NJ, USA). IHC staining was performed to analyze the C3 and IgG deposition in the kidneys.

2.7. Construction and treatment of pristane-induced lupus-like mice

Female C57BL/6J mice aged five weeks were intraperitoneally injected with 500 μL pristane (P2870, Sigma−Aldrich, St. Louis., MO, USA) per mouse. Fifteen weeks later, mice were given a booster shot with 500 μL pristane. Urine samples were collected from the pristane-treated mice, and urinary protein (Upro) levels were assessed by a colorimetric assay strip (URIT). The serum samples of pristane-treated mice were collected, and serum anti-dsDNA IgG levels were detected using ELISA. At 23 weeks, pristane-treated mice were divided into five groups according to Upro levels and serum anti-dsDNA IgG levels ($n = 11-12$ per group). Mice in the TP group were intraperitoneally injected with 0.05 mg/kg TP thrice weekly. Mice in the TP-PEG group were intraperitoneally injected with 0.375 mg/kg TP-PEG thrice weekly, maintaining the same molar amount as TP. According to the average DAR value of ADC-TP (4.75), mice in the ADC-TP group were intraperitoneally injected with 4.4 mg/kg ADC-TP three times per week, maintaining the same molar amount as TP-PEG. Mice in the CD19 mAb group were intraperitoneally injected with 4.4 mg/kg CD19 mAb thrice weekly, maintaining the same amount of CD19 mAb as ADC-TP. The serum samples of pristane-treated mice were collected at the beginning and end of the observation period. The serum anti-dsDNA IgG levels were detected by ELISA. Spleens were used to execute immune cell analysis by flow cytometry. IHC staining was performed to analyze the C3 and IgG deposition in the kidneys.

2.8. Long-term toxicity study

After one week of adaptive feeding, female ICR mice aged six weeks were divided into five groups according to body weight ($n = 6$ per group). Mice in the TP group were intraperitoneally injected with 0.05 mg/kg TP thrice weekly. Mice in the TP-PEG

group were intraperitoneally injected with 0.375 mg/kg TP-PEG thrice weekly, maintaining the same molar amount as TP. According to the average DAR value of ADC-TP (4.75), mice in the ADC-TP group were intraperitoneally injected with 4.4 mg/kg ADC-TP three times per week, maintaining the same molar amount as TP-PEG. Mice in the CD19 mAb group were intraperitoneally injected with 4.4 mg/kg CD19 mAb thrice weekly, maintaining the same amount of CD19 mAb as ADC-TP. Body weight and serum ALT and AST levels were monitored every three weeks. After treatment with these agents for 27 weeks, mice were sacrificed, and organs, as indicated, were collected for further analyses.

2.9. Western blot

Western blot was performed as previously described[35,36]. Primary antibodies used in Western blot are listed below. Anti-AKT (AF6261), anti-p70 S6k (AF6226), and anti-eIF2α (AF6087) antibodies were purchased from Affinity Biosciences (Ohio, USA). Anti-phospho-AKT (Ser473) (4060), anti-phospho-p70 S6k (Thr421/Ser424) (9204), PARP (9532), Caspase 3 (9662), Caspase 9 (9502), anti-phospho-eIF2α (Ser51) (3398) antibodies were purchased from Cell Signaling Technology (Boston, MA, USA). Anti-PGGT1B (ab122122) antibody was purchased from Abcam (Cambridge, UK). Anti-BAX (50599-2-Ig), anti-RAB14 (15662-1-AP), anti-GAPDH (10494-1-AP), anti- Bcl2 (68103-1-Ig) antibodies were purchased from ProteinTech Group (Wuhan, China).

2.10. Histological analysis

Tissues were fixed by paraformaldehyde, of which the concentration was 4%, and then embedded in paraffin. Sliced sections of 5 μm thickness were affixed into HistoBond® adhesive microscopic slides. These slides were stained with H&E (hematoxylin and eosin) and then stored at room temperature. For the immunofluorescence (IF) assay, slides were incubated at 70 °C for 1 h to dissolve the wax. The slides were further dewaxed by following sequential incubation: xylene for 10 min, 95% ethanol for 15 min, and 70% ethanol for 15 min. Then, the slides were incubated in a blocking buffer (5% FBS in PBST) for 30 min at room temperature. Sections were incubated with primary and secondary antibodies at 4 °C overnight and 30 min, respectively. The following antibodies were used: FITC-conjugated goat anti-mouse IgG2a heavy chain (ab97244, Abcam, Cambridge, UK), rat anti-mouse to C3[11H9] (ab11862, Abcam), and rhodamine goat anti-rat IgG (H + L) (AS022, ABclonal, Wuhan, China). The mouse kidneys' immune-complex (IC) depositions were analyzed and evaluated using a digital fluorescence microscope (OLYMPUS).

2.11. IC$_{50}$ measurement

Cells were treated with corresponding agents with various concentrations for 12 or 48 h, and cell viability was detected by MTT (C0009M, Beyotime) assay. Dose-response curves were fitted by GraphPad Prism 9 software. Then, IC$_{50}$ values were calculated.

2.12. Flow cytometry of dLNs and spleen tissues

dLNs and spleen tissues were ground and filtered to obtain a single-cell suspension. Approximately 1×10^6 cells were suspended in PBS and incubated with mouse Fc-R block (101302, Biolegend, San Diego, CA, USA) at room temperature for 10 min

and then incubated with fluorescent dye-conjugated antibodies against surface markers at 4 °C for 45 min in the dark. Cells were fixed and permeabilized for intracellular staining with a Transcription Factor Buffer Set (562574, BD Pharmingen) and then stained with fluorescent dye-conjugated antibodies for 1 h at 4 °C in the dark. The following fluorescent dye-conjugated antibodies were used in this study: Zombie Aqua (423102, Biolegend); Zombie NIR (423106, Biolegend); FITC-conjugated anti-CD3 antibody (100204, Biolegend); PerCP/Cyanine5.5-conjugated anti-CD4 antibody (116012, Biolegend); FITC-conjugated anti-CD4 antibody (553047, BD Pharmingen); APC/Cyanine7-conjugated anti-CD8 antibody (557654, BD Pharmingen); BV421-conjugated anti-CD44 antibody (563970, BD Pharmingen); FITC-conjugated anti-CD44 antibody (103022, Biolegend); PE/Cyanine7-conjugated anti-CD62L antibody (560516, BD Pharmingen); Biotin-conjugated anti-CXCR5 antibody (551960, BD Pharmingen); APC-conjugated anti-PD-1 antibody (562671, BD Pharmingen); BV711-conjugated anti-CD19 antibody (115555, Biolegend); PE-conjugated streptavidin (554061, BD Pharmingen); BV605-conjugated anti-B220 antibody (103244, Biolegend); PE/Cyanine7-conjugated anti-CD38 antibody (102718, Biolegend); PE-conjugated anti-FAS antibody (152608, Biolegend); AF647-conjugated anti-GL-7 antibody (561529, BD Pharmingen); PerCP/Cyanine5.5-conjugated anti-IgD antibody (405710, Biolegend); BV421-conjugated anti-CD138 antibody (142508, Biolegend); APC/Cyanine7-conjugated anti-CD11b antibody (557657, BD Pharmingen); PE-conjugated anti-CD25 antibody (102008, Biolegend); APC-conjugated anti-FOXP3 antibody (17-5773-82, Invitrogen); APC-conjugated anti-IFN-γ antibody (554413, BD Pharmingen); PE-conjugated anti-IL-4 antibody (554389, BD Pharmingen); PE/Cyanine7-conjugated anti-IL-17A antibody (506922, Biolegend).

2.13. Living imaging

MRL/*lpr* mice in the onset stage (22 weeks) were randomly divided into three groups, namely the TP-Cy7 group, CD19 mAb-Cy7 group, and ADC-TP-Cy7 group, to investigate the CD19 mAb-mediated B cell targeting ability. Mice were injected intraperitoneally and recorded as 0 h. At 48 h after injection, the fluorescence signal distribution in mice was recorded using *in vivo* imaging systems (IVIS spectroscopy, PerkinElmer, Waltham, MA, USA). Then, mice were euthanized, and the hearts, livers, spleens, lungs, kidneys, lymph nodes, uterus, and ovaries were collected for imaging under the IVIS imaging system to observe the fluorescence intensity of each tissue.

2.14. Human blood samples

Human blood samples were collected from healthy donors. Human peripheral blood mononuclear cells (PBMCs) were freshly isolated by density gradient centrifugation. The isolated PBMCs were cultured in RPMI1640 with 10% FBS and 1% penicillin/streptomycin for further treatments.

2.15. Statistical analysis

Data were analyzed using the GraphPad Prism 9 software (San Diego, CA, USA). All data were expressed as the means $\pm$ standard error of the mean (SEM). Student's *t*-test and one-way ANOVA were used to calculate statistical significance. Significant differences were marked as $*P < 0.05$; $**P < 0.01$; $***P < 0.001$; n.s., not significant.

3. Results

3.1. Design, prepare, and characterize CD19 mAb-TP conjugate

Since the toxicity of TWHF is generally derived from the untargeted accumulation of the major diterpenoids of TWHF in organs and tissues[13], we hypothesized that reducing the cytotoxicity of the major diterpenoids of TWHF by chemical modification or increasing targeting of the major diterpenoids of TWHF to target cells by conjugation of mAbs could vastly reduce the toxicity of TWHF. Considering that reducing the cytotoxicity of the major diterpenoids of TWHF by chemical modification will also reduce their killing effect on target cells, while increasing the number of drug molecules to target cells by conjugating mAbs may compromise the loss of efficacy caused by chemical modification, we proposed to combine these two approaches. PEGylation is a commonly used chemical modification of drug molecules in clinical practice[37]. Thus, we intended to construct CD19 mAb-TP conjugate using PEG$_{2000}$-NHS as a non-cleavable linker. Initially, we obtained TP modified with PEG$_{2000}$-NHS (Fig. 1A and B). We compared the cytotoxicity between PEGylated TP and TP in human normal hepatocytes HL-7702 cells, Madin−Darby canine kidney (MDCK) cells, human Epstein−Barr virus-transformed B cell line GM12878 cells, murine pro-B cell line BAF3 cells, and human T-cell lymphoma cell line Jurkat cells. As shown in Fig. 1C, the IC$_{50}$ values of PEGylated TP were 5−10 times higher than those of TP in these cell lines, indicating that PEGylation reduced the cytotoxicity of TP. We then conjugated PEGylated TP to a mouse CD19 blocking mAb by covalently binding the NHS reactive group of PEGylated TP to the dissociating amino group (-NH2) of CD19 mAb (Fig. 1D), and we named the CD19 mAb-TP conjugate ADC-TP. The drug-to-antibody ratio (DAR), defined as the number of warheads conjugated per antibody, is an essential factor affecting ADC efficacy and safety. The DAR value 4.0 was well established for microtubule inhibitor ADC warheads in multiple clinically approved ADCs, demonstrating excellent clinical efficacy and human safety profiles[34,38]. As shown in Fig. 1E, CD19 mAb conjugated with 4 TP molecules was the primary structural form of ADC-TP, and the average DAR value of ADC-TP was 4.75.

3.2. ADC-TP is efficiently internalized after binding to CD19 and selectively targets CD19$^+$ B cells

To determine whether ADC-TP could efficiently deliver TP into target cells, we examined internalization kinetics after treating A20 cells, a mouse CD19-positive B-cell lymphoma cell line, with ADC-TP. We noticed that ADC-TP could be detected by an AF488-conjugated goat anti-rat IgG antibody as early as 2 h in A20 cells (Fig. 2A). In contrast, ADC-TP could not be detected in CD19-null mouse T lymphoma cells, EL4, at the corresponding time points (Fig. 2A). Consistently, we also observed that ADC-TP co-localized with lysosome in A20 cells at the early stage (2 h) of cellular uptake, suggesting that ADC-TP could enter cells smoothly and be deposited in lysosome to release PEGylated TP (Fig. 2B). In contrast, ADC-TP could not even be detected in EL4 cells until the late stages of observation (Fig. 2B). Furthermore,
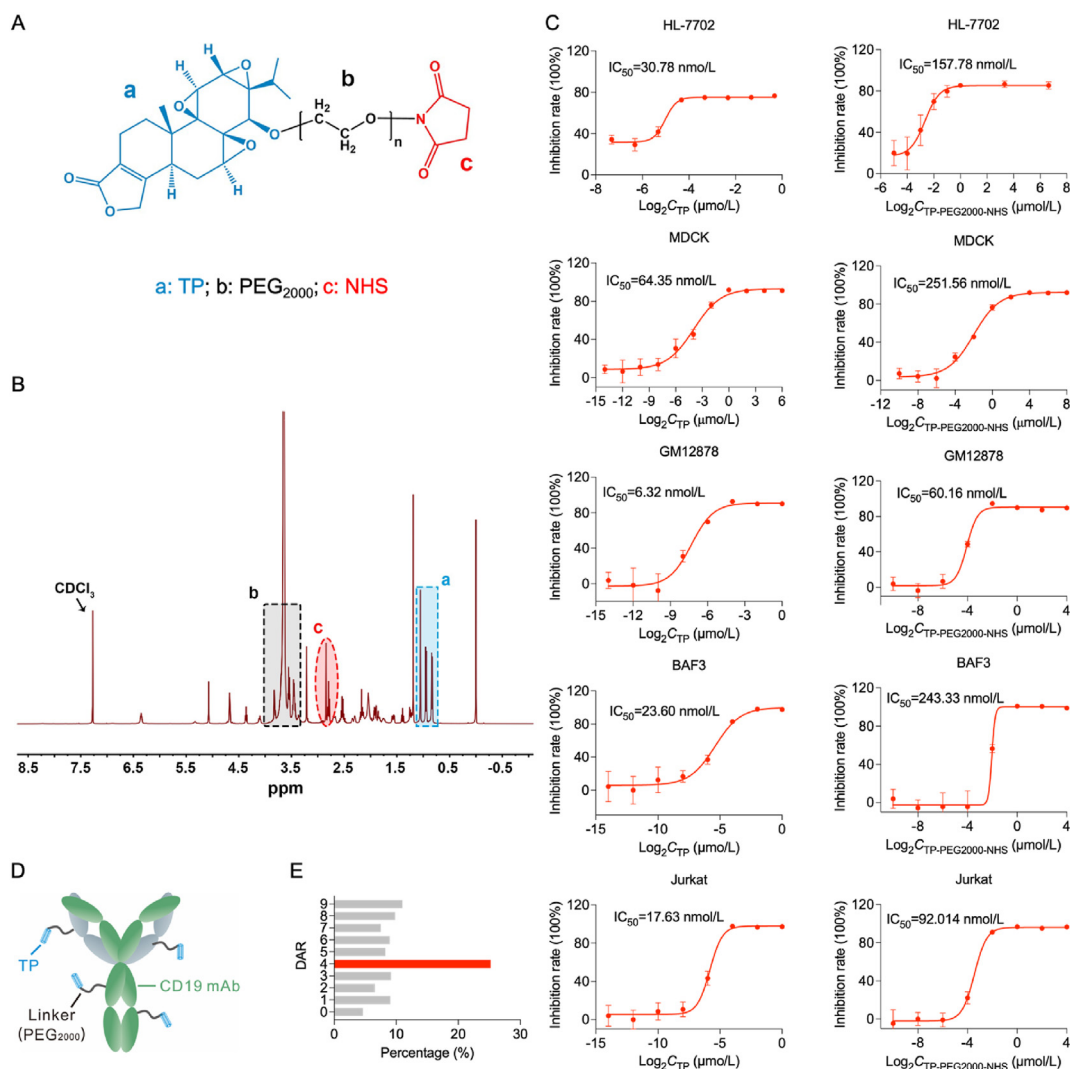
Figure 1 Construction and characterization of PEGylated TP and ADC-TP. (A) Chemical structure of TP-PEG$_{2000}$-NHS. (B) The synthesis of TP-PEG$_{2000}$-NHS was verified by ^{1}H NMR. (C) HL-7702, MDCK, GM12878, BAF3, and Jurkat cells were treated with TP or TP-PEG$_{2000}$-NHS with various concentrations for 48 h, and then an MTT assay was performed to detect cell viability. IC$_{50}$ curves were drawn using GraphPad Prism 9 software, and the IC$_{50}$ values were calculated ($n = 5-6$). (D) Structure diagram of CD19 mAb-TP conjugate ADC-TP. (E) DAR value distribution of ADC-TP. Data are represented as mean ± SEM.

we noted that the IC$_{50}$ values of TP were comparable in A20 cells (35.40 nmol/L) and EL4 cells (24.96 nmol/L) (Fig. 2C and D). The IC$_{50}$ value of PEGylated TP was increased in both A20 cells (315.1 nmol/L) and EL4 cells (405.8 nmol/L) (Fig. 2E and F), suggesting decreased cytotoxicity of PEGylated TP compared to TP. In addition, compared with PEGylated TP, ADC-TP showed a lower IC$_{50}$ value (57.83 nmol/L) in CD19-positive A20 cells but a significantly higher IC$_{50}$ value (296.3 nmol/L) in CD19-null EL4 cells (Fig. 2G and H), indicating that CD19 facilitated the uptake of ADC-TP. However, the difference between the two IC$_{50}$ values was less significant than expected; we thus analyzed CD19 expression in A20 and EL4 cells. We observed that EL4 cells had a particular expression of CD19 (Fig. 2I), which was much lower than that in A20 cells. To better characterize ADC-TP targeting to CD19, CD19 was forcedly expressed in Chinese hamster ovarian (CHO) cells, and its expression was validated by Western blot (Fig. 2J). TP, PEGylated TP, and ADC-TP cytotoxicity were detected in CD19$^+$ and CD19$^-$ CHO cells, respectively. We noted

that the IC$_{50}$ values of TP in CD19$^+$ CHO cells and CD19$^-$ CHO cells were 87.41 and 94.93 nmol/L, respectively (Fig. 2K and L), suggesting TP was toxic to both CD19$^+$ CHO cells and CD19$^-$ CHO cells. Consistently, the IC$_{50}$ value of PEGylated TP in CD19$^+$ CHO cells (468.1 nmol/L) was comparable with that of CD19$^-$ CHO cells (397.8 nmol/L) (Fig. 2M and N). However, the killing ability of ADC-TP on CD19$^+$ CHO cells was significantly enhanced, with an IC$_{50}$ value of only 6.13 nmol/L (Fig. 2O), while the IC$_{50}$ value of ADC-TP was as high as 27.21 μmol/L in CD19$^-$ CHO cells (Fig. 2P). These data demonstrate that ADC-TP could be efficiently internalized after binding to CD19.

Next, we set out to study whether the rationally designed ADC-TP could selectively target CD19-positive B cells. As shown in Fig. 2Q, both TP and ADC-TP showed desirable inhibitory effects on total cell viability of primary mouse splenic B cells, whereas ADC-TP was more potent than TP. Consistently, TP and ADC-TP decreased the frequency of CD19$^+$ B cells, and the efficacy of ADC-TP was better than that of TP (Fig. 2R). Inversely,
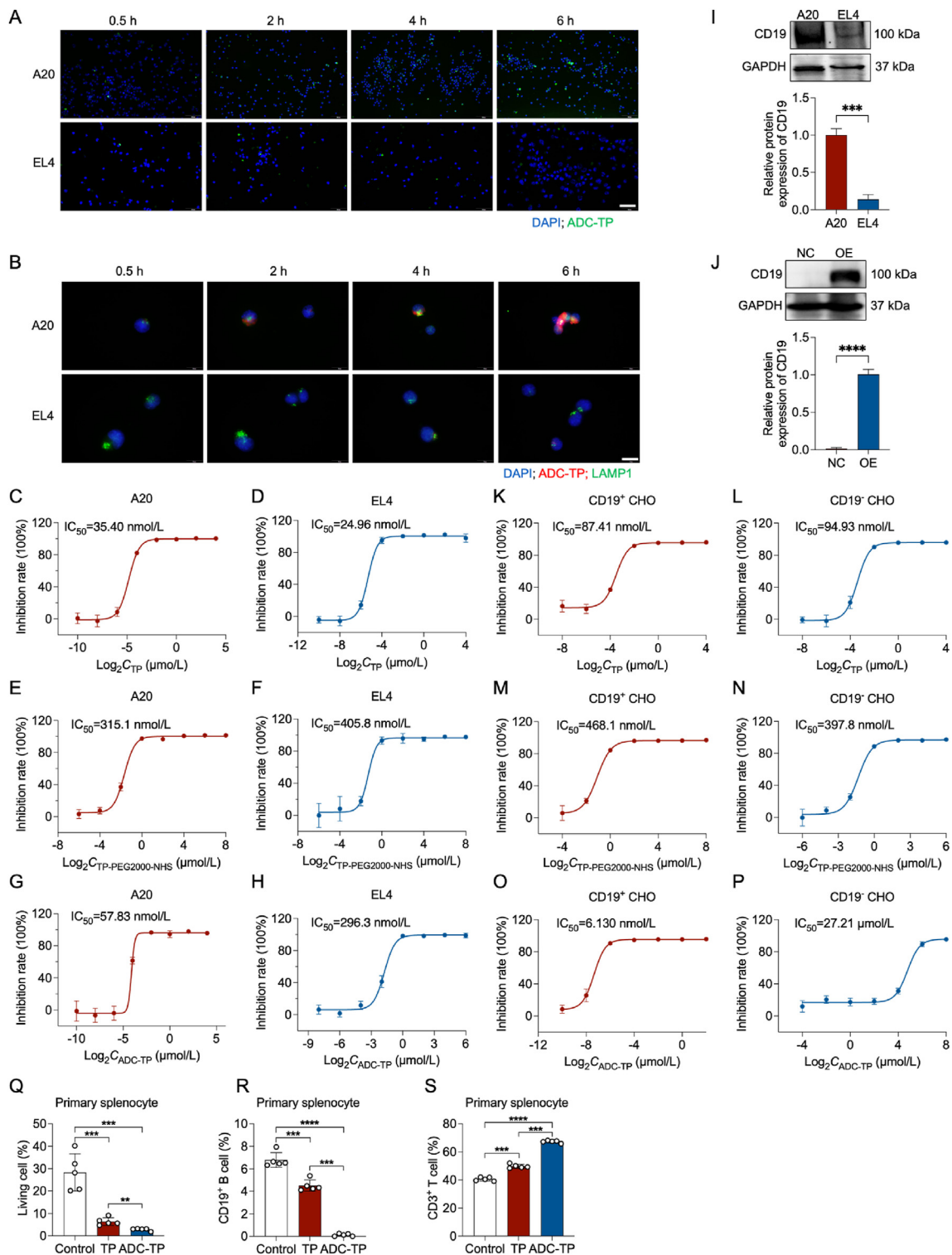
Figure 2 ADC-TP is efficiently internalized after binding to CD19 and selectively targets CD19$^+$ B cells. (A) Time-dependent images of A20 and EL4 cells that were pretreated with ADC-TP. Scale bar = 100 μm. (B) Time-dependent images of A20 and EL4 cells that were pretreated with ADC-TP. Scale bar = 20 μm. (C−H) CD19$^+$ A20 B cells and CD19$^-$ EL4 T cells were treated with TP, PEGylated TP, and ADC-TP with various concentrations for 12 h, and then an MTT assay was performed to detect cell viability. IC$_{50}$ curves were drawn using GraphPad Prism 9 software, and the IC$_{50}$ values were calculated (n = 6). (I) The CD19 protein expression in A20 and EL4 cells was analyzed by Western blot, with GAPDH as the loading control. (J) CHO cells were transfected with mouse CD19-expressing plasmid for 48 h; the CD19 protein expression was analyzed by Western blot, with GAPDH as the loading control. (K−P) CD19$^+$ CHO cells and CD19$^-$ CHO cells were treated with TP, PEGylated TP, and ADC-TP with various concentrations for 12 h, and then an MTT assay was performed to detect cell viability. IC$_{50}$ curves were drawn using GraphPad Prism 9 software, and the IC$_{50}$ values were calculated (n = 6). (Q−S) Primary mouse splenocytes were treated with 50 nmol/L TP and 10 nmol/L ADC-TP for 48 h; the frequencies of living cells (Q), CD19$^+$ B cells (R), and CD3$^+$ T cells (S) were analyzed by flow cytometry (n = 5). Data are represented as mean ± SEM. Statistical analysis was performed with one-way ANOVA. $**P < 0.01$; $***P < 0.001$; $****P < 0.0001$.

TP and ADC-TP increased the frequency of $CD3^+$ T cells, and the efficacy of ADC-TP was consistently better than that of TP (Fig. 2S). Hence, these data strongly suggest that ADC-TP could selectively target $CD19^+$ B cells.

3.3. Pharmacological and toxicological evaluation of ADC-TP in lupus-prone MRL/lpr mice

Next, we evaluated the therapeutical potential of ADC-TP in spontaneous lupus-prone MRL/*lpr* mice. Compared with MRL/MpJ control mice, MRL/*lpr* mice developed skin lesions characterized by redness, swelling, and ulceration. At the same time, ADC-TP significantly alleviated this symptom, which was also reflected by the reduction of the thickness of stratum corneum and inflammatory cell infiltration in hematoxylin and eosin (HE) staining of back skin tissues (Fig. 3A). The size and total cell numbers of the spleens were significantly reduced by ADC-TP treatment, which was more efficient than TP, TP-PEG (namely previously mentioned TP-PEG$_{2000}$-NHS) and CD19 mAb (Fig. 3B, Supporting Information Figs. S1 and S2A). Similarly, the size and total cell numbers of lymph nodes (LNs) were also significantly decreased by ADC-TP treatment (Fig. 3C and Supporting Information Fig. S3A). In addition, ADC-TP treatment had a significant renal protective effect, manifested by a decrease in urine protein (Upro) levels and blood urea nitrogen (BUN) levels (Fig. 3D and E). Consistent with this, HE staining showed swollen glomeruli and inflammatory cell infiltration in the kidneys from MRL/*lpr* mice, which was obviously ameliorated by ADC-TP treatment (Fig. 3F and G). Consistently, IgG&C3 immunofluorescent staining showed that ADC-TP treatment reduced the deposition of IgG and C3 in the glomeruli (Fig. 3F). Notably, the levels of serum anti-double strand DNA (anti-dsDNA) antibodies, one of the most important biomarkers for SLE diagnosis, was lower in ADC-TP treatment group (Fig. 3H). Subsequently, the spleens and draining LNs (dLNs) were analyzed by flow cytometry. Excitingly, the frequencies and numbers of $B220^+$ B cells in the spleens and dLNs were both significantly reduced by ADC-TP treatment (Fig. 3I and J, Figs. S2B and S3B). The numbers of $CD19^+$ B cells in the spleens and dLNs were also dramatically reduced (Figs. S2C and S3C). These results strongly support that ADC-TP could efficiently mitigate lupus symptoms by depleting B cells. We also analyzed the effects of these treatments on various subsets of immune cells by flow cytometry using gating strategies shown in Fig. S1. Upon ADC-TP treatment, the frequencies of splenic naïve B cells and memory B cells were not obviously changed, but the numbers of splenic naïve B cells and memory B cells both show a decreasing trend (Fig. S2D−S2G). Although there was no significant change in the proportion of germinal center (GC) B cells, its number showed a decreasing trend (Fig. S2H and L). Further analysis showed that these treatments did not induce any changes in the frequencies and numbers of antibody-secreting cells (ASCs), plasmablasts, and plasma cells (PCs) in the spleens (Fig. S2I−S2K and Fig. S2M−S2O). Consistently, these treatments did not show significant differences in the frequency and number of naïve B cells in dLNs (Figs. S3D and S3F). Although the frequency of memory B increased after ADC-TP treatment, the number actually decreased compared to the model group in dLNs (Figs. S3E and S3G). In addition, all these treatments did not influence the frequencies of GC B cells, ASCs, plasmablasts, and PCs in dLNs (Fig. S3H−S3K), and the cell numbers of GC B cells, ASCs, plasmablasts, and PCs in dLNs were also not be influenced by TP, TP-PEG and CD19 mAb (Fig. S3L−S3O). Meanwhile, ADC-TP decreased the cell numbers of GC B cells and ASCs and trended to reduce the cell numbers of plasmablasts in dLNs, but ADC-TP

ultimately did not affect the number of PCs (Fig. S3L−S3O). For $CD4^+$ T cell subsets, we noticed that ADC-TP increased the frequency of $CD4^+$ T cells in both spleens and dLNs (Supporting Information Figs. S4A and S5A). Furthermore, ADC-TP reduced the proportion of naïve T in spleens but did not significantly impact the proportion of naïve T in dLNs (Figs. S4B and S5B). However, these treatments showed no effects on the frequencies of effector T cells and central memory T cells in both spleens and dLNs (Figs. S4C, S4D and S5C, S5D). ADC-TP showed no noticeable effect on the number of $CD4^+$ T cells in the spleens but decreased the number of $CD4^+$ T cells in dLNs (Figs. S4E and S5E). In addition, ADC-TP decreases the number of naïve T cells, effector T cells, and central memory T cells in both spleens and dLNs (Figs. S4F−S4H and S5F−S5H). Further analysis showed that ADC-TP decreased the frequencies of splenic Tfh cells without affecting the splenic Th1, Th2, Th17, and Treg cells (Fig. S4I−S4M). The number of splenic Tfh significantly decreased, and there is a decreasing trend in the numbers of splenic Th1, Th2, Th17, and Treg cells in the ADC-TP group (Fig. S4N−S4R). In dLNs, ADC-TP reduced the frequency of Tfh cells and increased the frequency of Th2, Th17, and Treg cells while showing no effects on the frequencies of Th1 cells (Fig. S5I−S5M). The number of Tfh cells in dLNs was reduced after ADC-TP treatment, while the numbers of Th1, Th2, Th17, and Treg cells in dLNs were not influenced by ADC-TP treatment (Fig. S5N−S5R). These findings suggest that ADC-TP inhibits GC B cells and Tfh cells in MRL/*lpr* mice.

Of note, ADC-TP treatment had no noticeable effect on the body weight, suggesting that ADC-TP did not cause systemic toxicity in MRL/*lpr* mice (Fig. 3K). Moreover, the liver coefficient of MRL/*lpr* mice was increased, and ADC-TP treatment reduced the liver coefficient (Fig. 3L). The results of HE staining might explain this finding, as the infiltration of inflammatory cells in the liver of MRL/*lpr* mice increased, and ADC-TP treatment significantly alleviated this lesion (Fig. 3M). Consistently, serum ALT (alanine aminotransferase) levels of MRL/*lpr* mice tended to increase compared with that of MRL/MpJ mice, and ADC-TP treatment suppressed this increasing trend (Fig. 3N). Notably, serum AST (aspartate aminotransferase) levels of MRL/*lpr* mice were significantly increased compared to that of MRL/MpJ mice, and ADC-TP treatment significantly decreased it (Fig. 3O). These data indicated a spontaneous inflammatory liver injury of MRL/*lpr* mice, and ADC-TP treatment ameliorated the liver injury of MRL/*lpr* mice. Meanwhile, these data also suggest that this lupus-prone mice model is unsuitable for evaluating possible hepatotoxicity induced by ADC-TP. Besides, the organ coefficients of the uterus and ovaries of mice did not change (Fig. 3P). However, we observed a reduction in the number of growing and mature follicles in the cortex of ovarian tissue after TP treatment. In contrast, ADC-TP treatment did not affect the number and growth of follicles (Fig. 3Q). In addition, a small number of necrotic and exfoliated epithelial cells were observed in the uterine tissue after TP treatment but was not found in the group with ADC-TP treatment (Fig. 3Q). Collectively, these data suggest that ADC-TP possesses better therapeutical effect than TP with less influence on the reproductive system.

3.4. Pharmacological and toxicological evaluation of ADC-TP in pristane-induced lupus-like mice

To further confirm these findings observed in MRL/*lpr* mice, we evaluated the therapeutical efficacy and toxicity of ADC-TP in
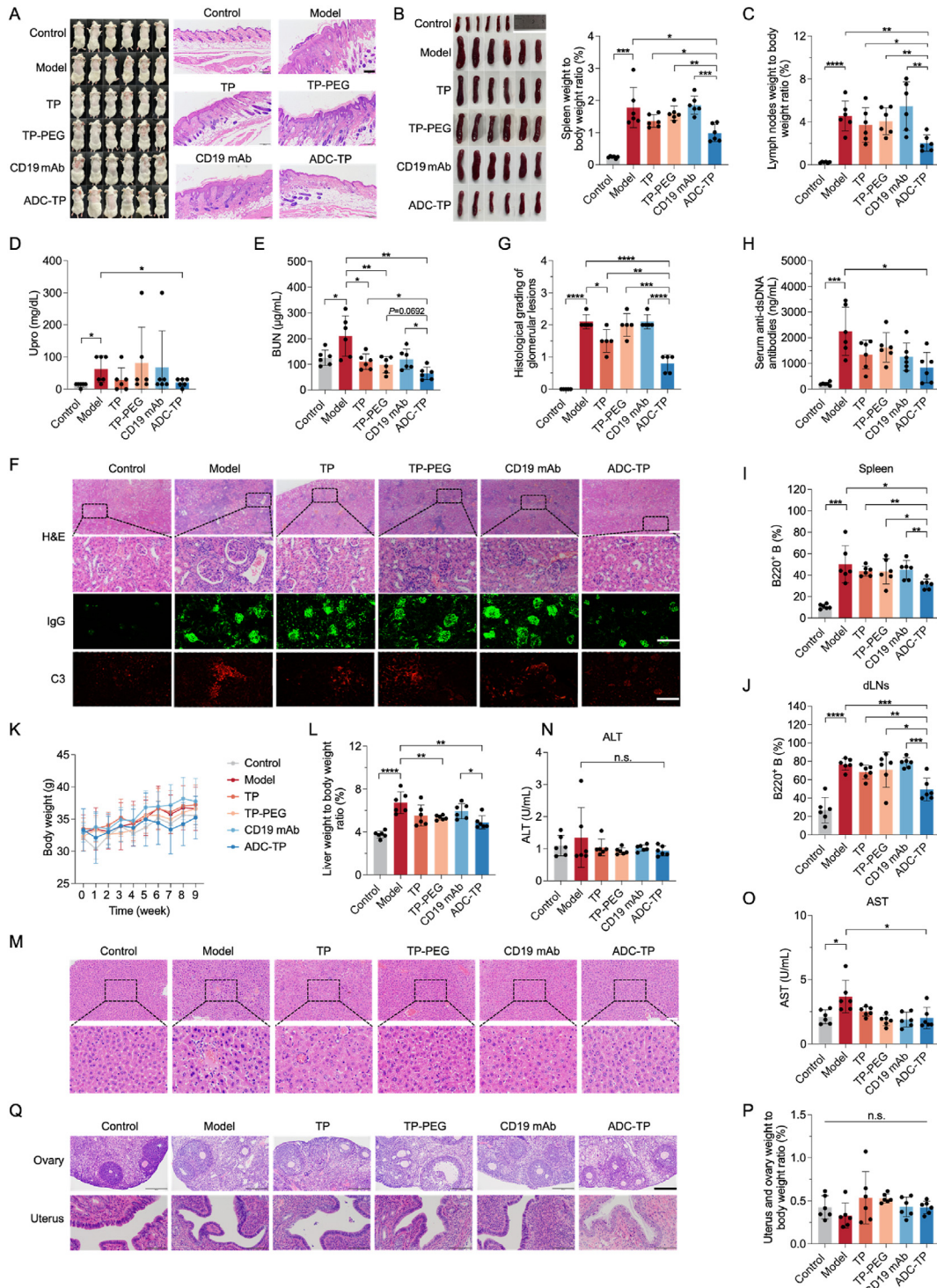
Figure 3 ADC-TP mitigates disease activity in lupus-prone MRL/*lpr* mice. Female MRL/*lpr* mice at the age of 16 weeks were equally divided into five groups according to basic Upro levels and serum anti-dsDNA levels, with MRL/MpJ mice at the same age as negative control ($n = 6$ for each group). After administration of TP, TP-PEG, CD19 mAb, and ADC-TP, as mentioned in the Materials and methods part, mice were sacrificed, and tissues, as indicated below, were collected for further analysis. (A) Pictures of back skin and representative pictures of HE staining of back skin tissues. Scale bar = 200 μm. (B) Pictures and organ coefficient of spleens ($n = 6$). (C) Organ coefficient of dLNs ($n = 6$). (D) Upro levels ($n = 6$). (E) Serum BUN levels ($n = 6$). (F) Representative pictures of HE staining, IgG, and C3 immunofluorescent staining of kidneys. Scale bars = 200 μm. (G) Renal pathological score ($n = 6$). (H) Serum anti-dsDNA levels ($n = 6$). (I) The frequency of splenic B220^{+} B cells ($n = 6$). (J) The frequency of B220^{+} B cells in dLNs ($n = 6$). (K) Body weight curve ($n = 6$). (L) Organ coefficient of the liver ($n = 6$). (M) Representative pictures of HE staining of livers. Scale bar = 100 μm. (N) Serum ALT levels ($n = 6$). (O) Serum AST levels ($n = 6$). (P) Organ coefficient of uterus and ovary ($n = 6$). (Q) Representative pictures of HE staining of the uterus and ovary. Scale bar = 200 μm. Data are represented as mean ± SEM. Statistical analysis was performed with one-way ANOVA. *$P < 0.05$; **$P < 0.01$; ***$P < 0.001$; ****$P < 0.0001$; n.s., not significant.

pristane-induced lupus-like mice compared with treatment with TP, TP-PEG, and CD19 mAb (Fig. 4A). After treatment for 12 weeks, we did not observe a change of body weight (Fig. 4B). Excitingly, ADC-TP was sufficient to decrease serum anti-dsDNA levels while TP, TP-PEG, and CD19 mAb showed no effect on it (Fig. 4C). Consistently, ADC-TP also reduced Upro levels, and although the difference did not reach statistical significance, it was still superior to TP, TP-PEG,

and CD19 mAb treatments (Fig. 4D). HE staining of the kidney showed that ADC-TP was able to mitigate inflammatory cell infiltration in the glomeruli, while TP, TP-PEG and CD19 mAb were less effective (Fig. 4E). Further, IgG and C3 immunofluorescent staining showed that ADC-TP treatment reduced the deposition of IgG and C3 in the glomeruli and the efficacy was more potent than TP, TP-PEG, and CD19 mAb treatments (Fig. 4F). Interestingly, although these
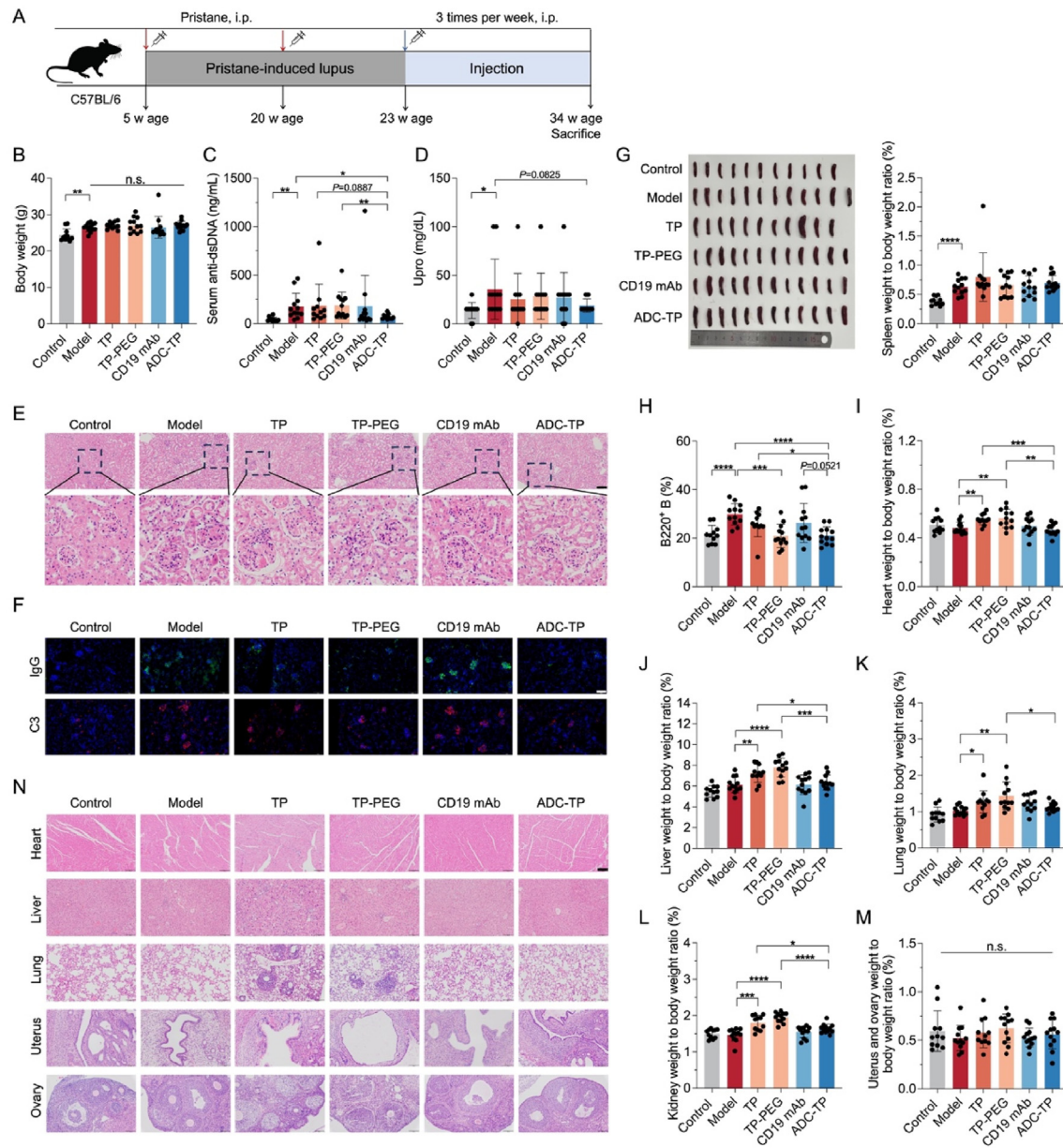

Figure 4 ADC-TP ameliorates murine lupus nephritis in pristane-induced lupus-like mice. 59 female C57BL/6J mice at the age of 5 weeks were injected with pristane as indicated to establish a lupus-like model with 11 untreated mice as normal control. Then, pristane-induced lupus-like mice were divided into five groups according to Upro levels and serum anti-dsDNA levels ($n = 11-12$ for each group). After administration of TP, TP-PEG, CD19 mAb, and ADC-TP, as mentioned in the Materials and methods part, mice were sacrificed, and tissues, as indicated below, were collected for further analysis. (A) Experimental schedule. (B) Body weight ($n = 11-12$). (C) Serum anti-dsDNA levels ($n = 11-12$). (D) Upro levels ($n = 11-12$). (E) Representative pictures of HE staining of kidneys. Scale bar = 200 μm. (F) Representative pictures of IgG and C3 immunofluorescent staining of kidneys. Scale bar: 100 μm. (G) Pictures and organ coefficient of the spleen ($n = 11-12$). (H) The frequency of splenic B220$^+$ B cells ($n = 11-12$). (I−M) Organ coefficient of the heart (I), liver (J), lung (K), kidney (L), uterus, and ovary (M) ($n = 11-12$). (N) Representative pictures of HE staining of the heart, liver, lung, uterus, and ovary. Scale bar = 100 μm. Data are represented as mean ± SEM. Statistical analysis was performed with one-way ANOVA. *$P < 0.05$; **$P < 0.01$; ***$P < 0.001$; ****$P < 0.0001$; n.s., not significant.

treatments did not reduce the size of the spleens (Fig. 4G), we did note a significant decline of the frequency of B220$^+$ B cells in the spleens upon TP-PEG and ADC-TP treatments (Fig. 4H). In addition, ADC-TP effectively reduced the ratio of splenic CD19$^+$ B cells, with better efficacy than TP and CD19 mAb (Supporting Information Fig. S6A). Further analysis showed that ADC-TP decreased the frequencies of splenic naïve B cells, memory B cells, and ASCs (Figs. S6B, S6C, and S6E), with an unexpected effect that increased the frequency of splenic GC B cells, plasmablasts, and PCs (Fig. S6D, S6F and S6G). Interestingly, the frequency of splenic CD4$^+$ T cells was increased after ADC-TP treatment (Fig. S6H), which might result from the dramatic decline of splenic CD19$^+$ B cells. However, there was no significant change in the proportion of CD8$^+$ T cells (Fig. S6I). Further analysis displayed that compared to TP, ADC-TP increased the frequency of splenic naïve T cells (Fig. S6J). ADC-TP had almost no effect on the proportion of effector T cells and effectively increased the proportion of central memory T cells (Figs. S6K and S6L). However, ADC-TP showed no effects on the frequencies of splenic Th1, Th2, Th17, and Tfh cells (Fig. S6M−S6P) but unexpectedly decreased the frequency of splenic Treg cells (Fig. S6Q). Hence, ADC-TP may act mainly through depleting B cells, with minor influence on CD4$^+$ T cells in the spleens from pristane-induced lupus-like mice. Comprehensively, these data suggest that ADC-TP effectively mitigated disease activity in pristane-induced lupus-like mice, and its therapeutical efficacy was superior to TP and CD19 mAb. In addition, we observed that TP and TP-PEG increased the organ coefficient of the heart, liver, lung, and kidney but had no influence on the organ coefficient of the uterus and ovary, while CD19 mAb and ADC-TP did not affect the organ coefficient of these organs (Fig. 4I−M). HE staining showed that TP and TP-PEG lead to increased inflammatory infiltration in the liver and lung, but no visible pathologic changes were found in the heart, uterus, and ovary (Fig. 4N). CD19 mAb and ADC-TP consistently did not induce any pathologic changes in these organs (Fig. 4N). It is noteworthy that although TP reduced renal inflammatory infiltration (Fig. 4E), it still increased the organ coefficient of the kidney (Fig. 4L). Taken together, these results demonstrate that ADC-TP is more effective and safer than TP and CD19 mAb in pristane-induced lupus-like mice.

3.5.   Long-term toxicity study of ADC-TP

Afterward, to study whether this rationally designed ADC-TP could cause cumulative toxicity, we carried out a long-term toxicity study of ADC-TP compared to TP, TP-PEG, and CD19 mAb. Female ICR mice were given these agents with equal molar TP for up to 27 weeks. We did not observe a body weight change during the long-term administration of ADC-TP, as well as TP, TP-PEG, and CD19 mAb (Fig. 5A). ADC-TP also did not increase serum ALT and AST levels (Fig. 5B and C). However, TP and TP-PEG significantly increased serum ALT and AST levels, and the magnitude of TP-PEG-induced increase of ALT was smaller than that of TP, suggesting that hepatotoxicity induced by TP-PEG was slighter than that caused by TP (Fig. 5B and C). Unexpectedly, CD19 mAb treatment also elevated serum ALT and AST levels (Fig. 5B and C). Further, although the organ coefficient of the liver was not changed by long-term administration of ADC-TP, TP, TP-PEG, and CD19 mAb (Fig. 5D), we observed that TP and TP-PEG treatment resulted in cellular swelling of the liver while ADC-TP treatment showed no effect on it (Fig. 5E). In addition, serum BUN levels and the organ coefficient of the kidney were not altered by long-term administration of ADC-TP, TP, TP-PEG and CD19 mAb (Fig. 5F and G). Consistently, HE staining of the

kidney also did not exhibit any pathological changes (Fig. 5H). Moreover, serum BUN levels and the organ coefficient of the uterus and ovary were also not altered by long-term administration of ADC-TP, TP, TP-PEG, and CD19 mAb (Fig. 5I and J). HE staining showed no morphological changes in the uterus and ovary (Fig. 5H). Besides, long-term administration of ADC-TP, TP, TP-PEG, and CD19 mAb had no effects on the organ coefficient of the lung, heart, and spleen (Fig. 5K−M). In summary, these results indicate that long-term use of ADC-TP is safe, and this is particularly important for SLE with long treatment periods.

3.6.   Reduced accumulation of ADC-TP in the liver, kidney, uterus and ovary

Next, we set out to analyze the mechanisms underlying ADC-TP improvement. As the side effects of TWHF or TP primarily derived from its untargeted accumulation in other organs, we determined the lymphoid tissue specificity and untargeted accumulation of ADC-TP in other organs in MRL/lpr mice. To visualize the distribution of TP, CD19 mAb, and ADC-TP in vivo, these agents were prelabeled with Cy7 and injected intraperitoneally into mice two times (Fig. 6A). As shown in Fig. 6B, TP-Cy7, CD19 mAb-Cy7, and ADC-TP-Cy7 all mainly accumulated in the abdominal cavity and some was observed in the neck. Excitingly, the accumulation of ADC-TP-Cy7 and CD19 mAb in the neck was increased than that of TP-Cy7 (Fig. 6B). For further analysis, the accumulation of TP-Cy7, CD19 mAb-Cy7, and ADC-TP-Cy7 in specific organs, mice were sacrificed and heart, liver, spleen, lung, kidney, LNs, uterus and ovary were harvested for visualization. The fluorescence imaging of in vitro tissues showed that TP-Cy7 mainly accumulated in the liver and kidney, but a considerable amount of TP-Cy7 also accumulated in the spleen, LNs, uterus, and ovary, and less accumulated in the heart and lung (Fig. 6C and D, Supporting Information Fig. S7A and S7B). Notably, the accumulation of CD19 mAb-Cy7 and ADC-TP-Cy7 in the liver, kidney, uterus, and ovary were decreased than that of TP-Cy7 (Fig. 6C, D, and Fig. S7C−S7E). In contrast, the accumulation of CD19 mAb-Cy7 and ADC-TP-Cy7 in LNs was markedly increased than that of TP-Cy7 (Fig. 6C, D, and Fig. S7F). Unexpectedly, the accumulation of CD19 mAb-Cy7 and ADC-TP-Cy7 in the spleens was comparable to that of TP-Cy7 (Fig. 6C, D, and Fig. S7G). Collectively, these data demonstrate that ADC-TP accumulates more in lymphoid tissues and less in the liver, kidney, uterus, and ovary compared with TP.

3.7.   ADC-TP triggers apoptosis, ERS and suppresses mTOR signaling in B cells

Next, we investigated whether ADC-TP retained the cytotoxic effect of TP. In A20 B cells, ADC-TP triggered apoptosis as TP did (Fig. 7A). At protein levels, ADC-TP increased the cleavage of PARP, Caspase 9 and Caspase 3, downregulated the expression of anti-apoptotic protein Bcl2 and upregulated the expression of pro-apoptotic protein BAX (Fig. 7B). In addition, ADC-TP inhibited the phosphorylation of p70 S6K and AKT, suggesting ADC-TP was able to suppress mTOR signaling, which is essential for cell proliferation and survival[39] (Fig. 7C). Surprisingly, ADC-TP and TP both increased the phosphorylation of eIF2α and ATF4 expression, indicating the induction of endoplasmic reticulum stress (ERS) by ADC-TP and TP (Fig. 7C). Furthermore, these findings were confirmed in primary splenic B cells (Fig. 7D). We also checked these findings in B220$^+$ B cells from dLNs of MRL/lpr mice and
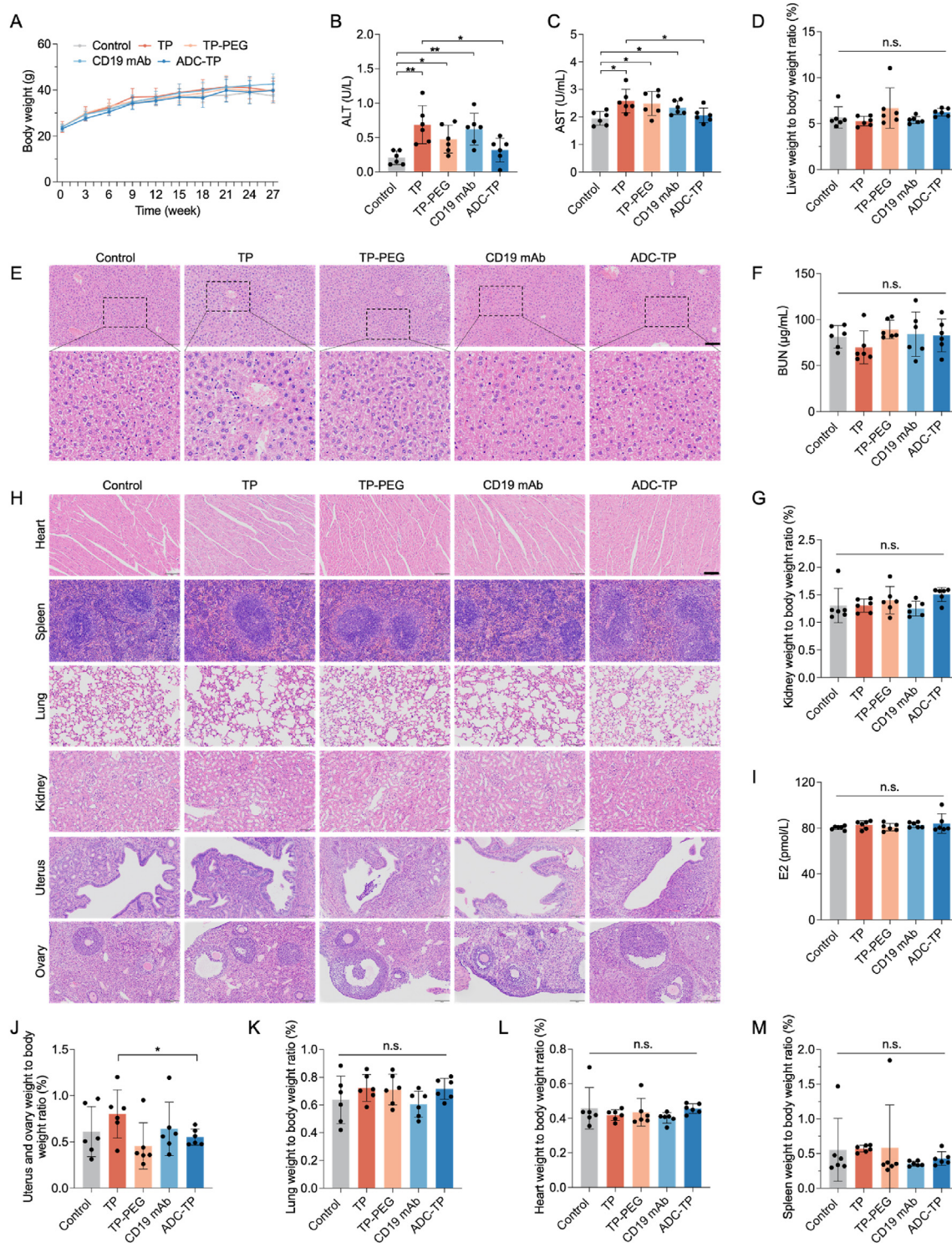
Figure 5 ADC-TP is safe in a long-term toxicity study. Female ICR mice at the age of 6 w were equally divided into five groups according to body weight ($n = 6$ for each group). After administration of TP, TP-PEG, CD19 mAb, and ADC-TP, as mentioned in the Materials and methods part, mice were sacrificed, and tissues, as indicated below, were collected for further analysis. (A) Body weight change curve. (B) Serum ALT levels ($n = 6$). (C) Serum AST levels ($n = 6$). (D) Organ coefficient of the liver ($n = 6$). (E) Representative pictures of HE staining of the liver. Scale bar $= 100$ μm. (F) Serum BUN levels ($n = 6$). (G) Organ coefficient of the kidney ($n = 6$). (H) Representative pictures of HE staining of the heart, spleen, lung, kidney, uterus, and ovary. Scale bar $= 100$ μm. (I) Serum E2 levels ($n = 6$). (J) Organ coefficient of the uterus and ovary ($n = 6$). (K) Organ coefficient of the lung ($n = 6$). (L) Organ coefficient of the heart ($n = 6$). (M) Organ coefficient of the spleen ($n = 6$). Data are represented as mean ± SEM. Statistical analysis was performed with one-way ANOVA. *$P < 0.05$; **$P < 0.01$; n.s., not significant.
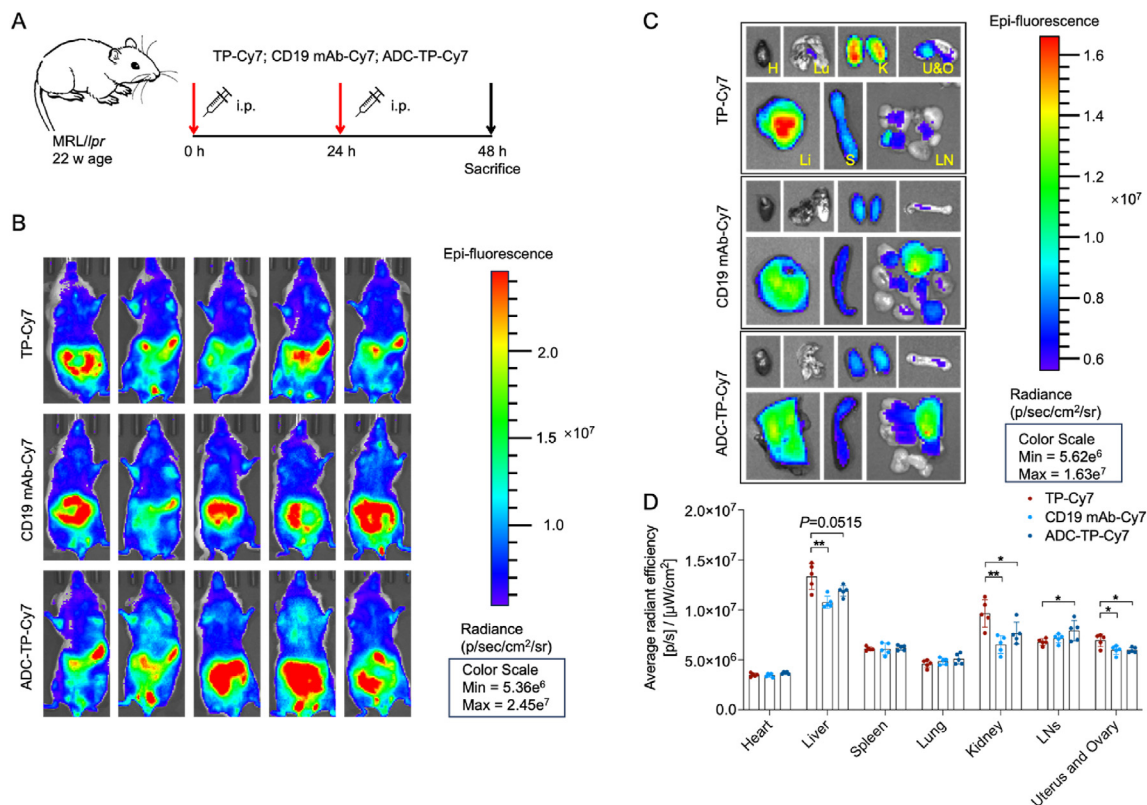
Figure 6 Biodistribution of ADC-TP in MRL/*lpr* mice. (A) Schematic design of TP-Cy7, CD19-Cy7, and ADC-TP-Cy7 biodistribution in MRL/*lpr* mice. (B) *In vivo* NIR fluorescent images of MRL/*lpr* mice at 48 h after administering TP-Cy7, CD19-Cy7, and ADC-TP-Cy7 ($n = 5$). (C) Representative *ex vivo* NIR fluorescent images of seven major organs, including heart (H), liver (L), spleen (S), lung (LU), kidney (K), lymph nodes (LN), uterus, and ovary (U&O). (D) Quantified normal organ distribution of TP-Cy7, CD19-Cy7, and ADC-TP-Cy7 ($n = 5$). Data are represented as mean $\pm$ SEM. Statistical analysis was performed with one-way ANOVA. *$P < 0.05$; **$P < 0.01$.

the spleens of pristane-induced lupus-like mice. As shown in Fig. 7E, ADC-TP increased the protein expression of BiP in B220$^+$ B cells from dLNs of MRL/*lpr* mice, indicating the induction of ERS in B220$^+$ B cells by ADC-TP treatment *in vivo*. Consistent with previous *in vitro* findings, ADC-TP treatment increased the cleavage of Caspase 3 and decreased the phosphorylation of S6 ribosomal protein in B220$^+$ B cells from the spleens of pristane-induced lupus-like mice, suggesting that the induction of apoptosis and inhibition of mTOR signaling after ADC-TP treatment (Fig. 7F and G). Hence, ADC-TP could act by inducing apoptosis and ERS and inhibiting mTOR signaling in B cells.

3.8. Human ADC-TPs selectively deplete B cells in PBMCs from healthy donors

To verify the feasibility of the ADC strategy in humans, we constructed two human ADC-TPs named ADC-TP (Den) and ADC-TP (Ine) by coupling PEGylated TP with two anti-human CD19 blocking mAbs, Denintuzumab (Den) and Inebilizumab (Ine), respectively. In addition, we constructed a control ADC-TP (IgG) using untargeted humanized IgG. We compared the efficacies of TP, TP-PEG, Den, Ine, ADC-TP (IgG), ADC-TP (Den), and ADC-TP (Ine) on killing B cell subsets in PBMCs from healthy donors. As one mouse CD19 mAb molecule conjugated at most nine TP molecules (Fig. 1E), we had reason to speculate that one human CD19 mAb molecule conjugated no more than 10 TP molecules. Thus, we treated human PBMCs with 100 nmol/L TP, 100 nmol/L

TP-PEG, 10 nmol/L ADC-TP (IgG), 10 nmol/L Den, 10 nmol/L Ine, 10 nmol/L ADC-TP (Den), and 10 nmol/L ADC-TP (Ine) for 48 h. As shown in Fig. 8A, 100 nmol/L TP and 100 nmol/L TP-PEG slightly reduced the frequency of CD19$^+$ B cells. 10 nmol/L Den, 10 nmol/L Ine, 10 nmol/L ADC-TP (Den), and 10 nmol/L ADC-TP (Ine) dramatically reduced the frequency of CD19$^+$ B cells. Notably, the efficacies of 10 nmol/L ADC-TP (Den) and 10 nmol/L ADC-TP (Ine) were better than 10 nmol/L Den and 10 nmol/L Ine, respectively. In addition, 100 nmol/L TP, 100 nmol/L TP-PEG, 10 nmol/L Den, 10 nmol/L ADC-TP (Den) and 10 nmol/L ADC-TP (Ine) increased the frequency of CD3$^+$ T cells (Fig. 8B). Unexpectedly, 10 nmol/L ADC-TP (IgG) decreased the frequency of CD3$^+$ T cells (Fig. 8B). Furthermore, although the efficacy of 10 nmol/L ADC-TP (Den) on increasing the frequency of CD3$^+$ T cells was comparable to that of 10 nmol/L Den, the efficacy of 10 nmol/L ADC-TP (Ine) on increasing the frequency of CD3$^+$ T cells was significantly better than that of 10 nmol/L Ine (Fig. 8B). Meanwhile, the efficacies of 10 nmol/L ADC-TP (Den) and 10 nmol/L ADC-TP (Ine) on increasing the frequency of CD3$^+$ T cells were both better than that of 100 nmol/L TP-PEG (Fig. 8B). Collectively, these results suggest that the ADC-TP strategy is effective in enhancing the efficacy of human CD19 mAbs and TP.

4. Discussion

In our present study, CD19 mAb-TP conjugate (ADC-TP) was designed to reduce the side effects of TP and improve the efficacy
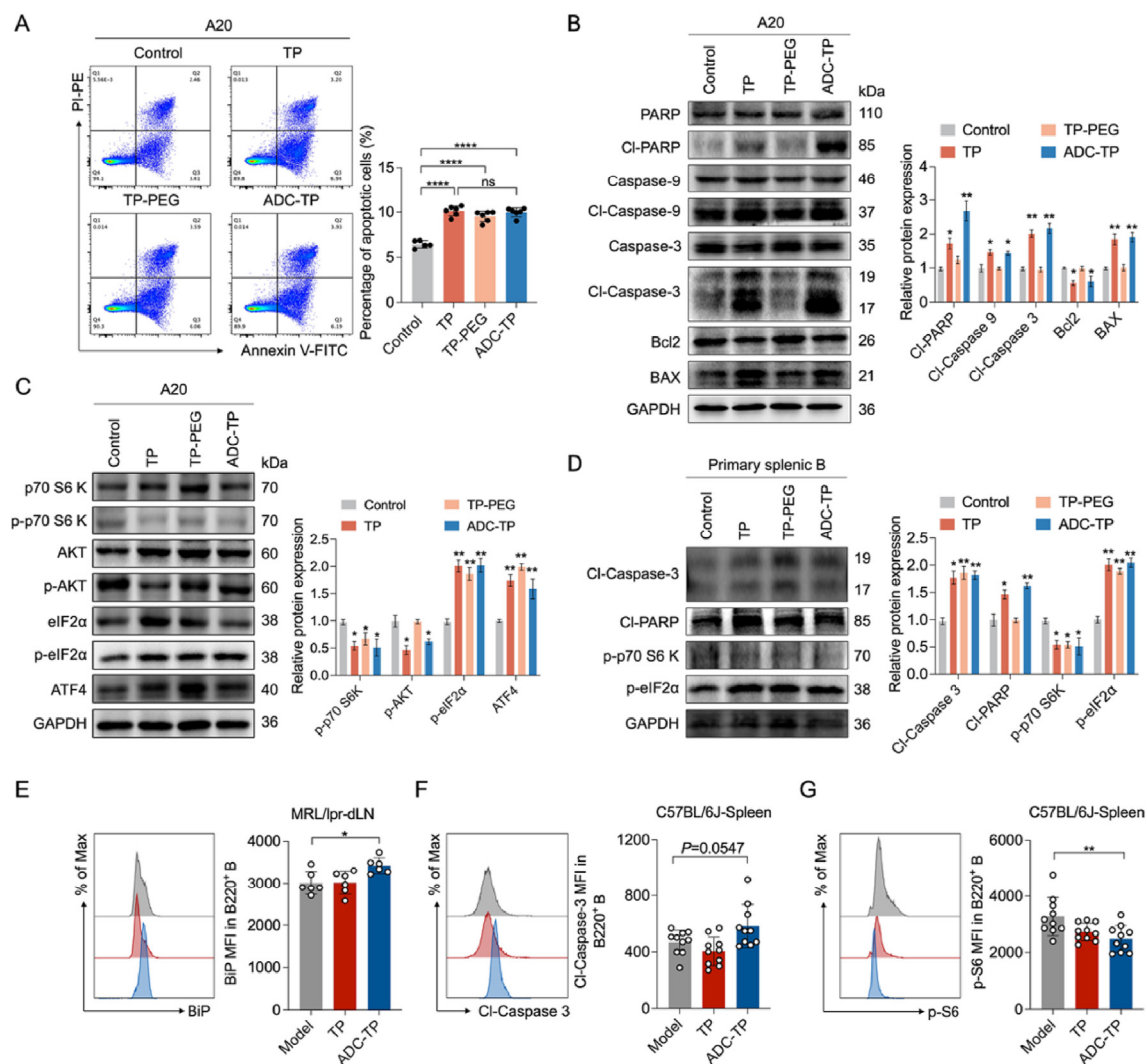
Figure 7 Mechanisms underlying the cytotoxicity of ADC-TP. (A) A20 cells were treated with 50 nmol/L TP, 50 nmol/L TP-PEG, and 10.5 nmol/L ADC-TP for 48 h, then cells were double-stained with Annexin V and PI, and the apoptotic rate was measured by flow cytometry (n = 5−6). (B, C) A20 cells were treated with 50 nmol/L TP, 50 nmol/L TP-PEG, and 10.5 nmol/L ADC-TP for 48 h, and the expression of indicated proteins was analyzed by Western blot, with GAPDH as the loading control (n = 3). (D) Primary mouse splenic B cells were treated with 50 nmol/L TP, 50 nmol/L TP-PEG, and 10.5 nmol/L ADC-TP for 48 h; the expression of indicated proteins was analyzed by Western blot, with GAPDH as the loading control (n = 3). (E) BiP expression in B220+ B cells from dLNs of MRL/*lpr* mice mentioned before was analyzed by flow cytometry (n = 6). (F, G) Cleaved-Caspase 3 and p-S6 expression in splenic B220+ B cells of pristane-induced lupus-like mice mentioned before was analyzed by flow cytometry (n = 11−12). Data are represented as mean ± SEM. Statistical analysis was performed with one-way ANOVA. *P < 0.05; **P < 0.01; ****P < 0.0001.

of CD19 mAb in the treatment of SLE. ADC-TP selectively depleted B cells *in vitro* and *in vivo*, effectively alleviating disease symptoms in two lupus mice models without causing side effects. Mechanistically, ADC-TP was accumulated in lymphatic tissues, and B cells were selectively eliminated by inducing apoptosis and ERS and suppressing the AKT-mTOR signaling pathway. Moreover, long-term administration of ADC-TP did not cause detectable toxicity. Thus, this study provides a feasible strategy for improving current agents for the treatment of SLE.

To date, our results provide the first experimental evidence of using the ADC strategy for enhancing the therapeutical efficacy of B cell-targeting mAbs and mitigating the side effects of cytotoxic agents used for the treatment of SLE. As we know, despite the rapid development of precision medicine in SLE, the current management of SLE still relies on immunosuppressants, such as cyclophosphamide (CTX) and methotrexate (MTX)[40]. However, although these immunosuppressants have shown impressive clinical efficacy in treating SLE, they may cause serious side effects due to their nonspecific targeting of other organs[41]. Thus, these immunosuppressants are well-suited to be improved by ADC strategies in future studies.

Currently, ADC drugs have achieved success only in cancer therapy. Thus far, there are fifteen approved ADC drugs worldwide, seven of which are for hematologic malignancies and target six different antigens, including CD33, CD30, CD22, CD79b, B-cell maturation antigen (BCMA/TNFRSF17), and CD19. The other eight ADC drugs have been approved for solid tumors by respectively targeting six different antigens, including HER2,
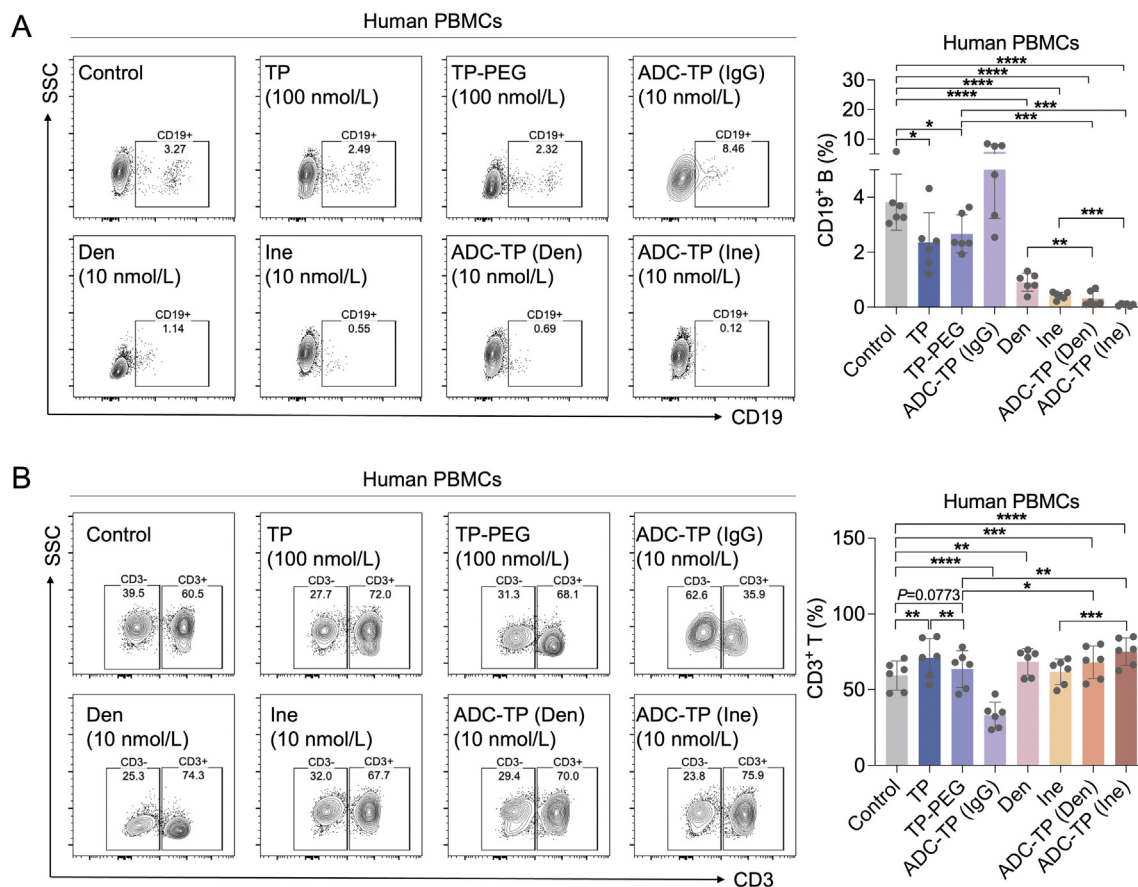
Figure 8 Human ADC-TPs show enhanced efficacies in depleting CD19$^+$ B cells from human PBMCs. (A, B) Human PBMCs were treated with 100 nmol/L TP, 100 nmol/L TP-PEG, 10 nmol/L ADC-TP (IgG), 10 nmol/L Den, 10 nmol/L Ine, 10 nmol/L ADC-TP (Den), and 10 nmol/L ADC-TP (Ine) for 48 h, the frequencies of CD19$^+$ B cells and CD3$^+$ T cells were analyzed by flow cytometry. Data are represented as mean ± SEM. Statistical analysis was performed with one-way ANOVA. $*P < 0.05$; $**P < 0.01$; $***P < 0.001$; $****P < 0.0001$.

Nectin-4, tumor-associated calcium signal transducer 2 (TROP2), tissue factor (TF), EGFR and folate receptor α (FRα)[42]. Theoretically, ADC can reduce the damage of chemotherapy drugs to normal cells and target the tumor cells expressing the antigen, and high doses of chemotherapy drugs can accurately kill tumor cells. However, most ADCs are still burdened by off-target toxicities that resemble those of the cytotoxic payload, as well as on-target toxicities and other poorly understood and potentially life-threatening adverse effects[43]. Thus, other improvement strategies can also be considered. Aptamers are single-stranded DNA or RNA sequences that can specifically bind with the target protein or molecule *via* specific secondary structures. Compared with ADC, aptamer−drug conjugate (ApDC) is a therapeutic strategy with a smaller size, higher chemical stability, lower immunogenicity, faster tissue penetration, and facile engineering, but lower *in vivo* specificity, serum stability, and quicker renal clearance[44]. A TP ApDC has been developed to treat triple-negative breast cancer (TNBC). Notably, the TP ApDC has excellent *in vivo* antitumor efficacy for TNBC and negligible side effects on healthy organs[45]. Therefore, TP ApDC is also an attractive approach for mitigating TP's "off-target"-induced toxicity. In addition, peptide drug conjugate (PDC) is a new type of drug conjugate. In contrast to ADC, it targets cells by a peptide chain of about ten amino acids, so it does not induce an immune response[46]. Therefore, in future studies, TP ADC, TP ApDC, and TP PDC in the context of lupus should be compared comprehensively.

There are also some limitations in our present study. Long-lived plasma cells (LLPCs) are recognized as the critical pathological basis for the relapse of refractory SLE, which are unresponsive to standard immunosuppression[47]. CD19 mAb-TP conjugates may not be able to solve the problem of LLPCs. Developing a dual-targeting mAb-TP conjugate of CD19 and plasma cell antigens such as CD38 and CD138 may significantly improve therapeutic efficacy. Most importantly, we constructed ADC-TP here using a mouse CD19 mAb to verify the feasibility of an ADC strategy in enhancing the therapeutic efficacy of B cell-targeting agents and alleviating the side effects of TWHF in mouse models. Future clinical trials need to test the exact efficacy of an ADC strategy.

5. Conclusions

In summary, this study presented a novel strategy to mitigate the toxicity of TWHF while enhancing the therapeutical efficacy of CD19 mAbs for the treatment of SLE. By conjugating CD19 mAb with PEGylated TP to construct a CD19 mAb-TP conjugate (ADC-TP), the therapeutic efficacies of both TP and CD19 mAb were enhanced, and the side effects of TP were largely

diminished. This was mainly because of the higher concentration of ADC-TP in lymphoid organs and the lower accumulation in the liver, kidney, uterus, and ovary. Thus, ADC-TP has great potential for clinical translation, and our study provides a feasible strategy for improving the current agents used to treat SLE.

Acknowledgments

Author contributions

Qianjin Lu and Ming Zhao proposed the concept of the project. Lai Wang designed the experiments. Haoyuan Yin and Jiao Jiang performed the experiments. Qilin Li completed the Western blot experiments. Changxing Gao performed animal imaging experiments. Wenrui Li, Bo Zhang, Yue Xin, and Hongyang Li analyzed the data. Lai Wang and Haoyuan Yin wrote the manuscript. All authors have read and approved the final version of the manuscript.

Conflicts of interest

The authors have no conflicts of interest to declare.

Appendix A.   Supporting information

Supporting information to this article can be found online at https://doi.org/10.1016/j.apsb.2024.06.024.

References

1. Tong L, Zhao QF, Datan E, Lin GQ, Minn I, Pomper MG, et al. Triptolide: reflections on two decades of research and prospects for the future. *Nat Prod Rep* 2021;**38**:843−60.
2. Ma J, Dey M, Yang H, Poulev A, Pouleva R, Dorn R, et al. Anti-in-flammatory and immunosuppressive compounds from *Tripterygium wilfordii*. *Phytochemistry* 2007;**68**:1172−8.
3. Chen Y, Wang YF, Song SS, Zhu J, Wu LL, Li XY. Potential shared therapeutic and hepatotoxic mechanisms of *Tripterygium wilfordii* polyglycosides treating three kinds of autoimmune skin diseases by regulating IL-17 signaling pathway and Th17 cell differentiation. *J Ethnopharmacol* 2022;**296**:115496.
4. Zhang J, Zeng YQ, Zhang J, Pan XD, Kang DY, Huang TW, et al. Tripchlorolide ameliorates experimental autoimmune encephalomy-elitis by down-regulating ERK1/2-NF-κB and JAK/STAT signaling pathways. *J Neurochem* 2015;**133**:104−12.
5. Meng HT, Zhu L, Ni WM, You LS, Jin J, Qian WB. Triptolide inhibits the proliferation of cells from lymphocytic leukemic cell lines in as-sociation with downregulation of NF-κB activity and miR-16-1*. *Acta Pharmacol Sin* 2011;**32**:503−11.
6. Zhao X, Tang XJ, Yan Q, Song H, Li ZT, Wang DD, et al. Triptolide ameliorates lupus *via* the induction of miR-125a-5p mediating Treg upregulation. *Int Immunopharmacol* 2019;**71**:14−21.
7. Fu JM, Zang YD, Zhou Y, Chen CJ, Shao S, Shi GN, et al. Exploring a novel triptolide derivative possess anti-colitis effect *via* regulating T cell differentiation. *Int Immunopharmacol* 2021;**94**:107472.
8. Hu YQ, Wu QG, Wang YL, Zhang HB, Liu XY, Zhou H, et al. The molecular pathogenesis of triptolide-induced hepatotoxicity. *Front Pharmacol* 2022;**13**:979307.
9. Lu J, Zhang Y, Dong HY, Sun JJ, Zhu L, Liu PY, et al. New mecha-nism of nephrotoxicity of triptolide: oxidative stress promotes cGAS-STING signaling pathway. *Free Radic Biol Med* 2022;**188**:26−34.
10. Ge JC, Qian Q, Gao YH, Zhang YF, Li YX, Wang X, et al. Toxic effects of *Tripterygium* glycoside tablets on the reproductive system of male rats by metabolomics, cytotoxicity, and molecular docking. *Phytomedicine* 2023;**114**:154813.
11. Huang L, Feng S, Wang H. Decreased bone mineral density in female patients with systemic lupus erythematosus after long-term administration of *Tripterygium wilfordii* Hook. F. *Chin Med J Engl* 2000;**113**:159−61.
12. Ren Q, Li MM, Deng Y, Lu AP, Lu J. Triptolide delivery: nanotechnology-based carrier systems to enhance efficacy and limit toxicity. *Pharmacol Res* 2021;**165**:105377.
13. Song J, He GN, Dai L. A comprehensive review on celastrol, triptolide and triptonide: insights on their pharmacological activity, toxicity, combination therapy, new dosage form and novel drug delivery routes. *Biomed Pharmacother* 2023;**162**:114705.
14. Sandoval-Heglund D, Roberts E, Park J, Dall'Era M, Lanata C, Barbour KE, et al. Economic insecurities and patient-reported out-comes in patients with systemic lupus erythematosus in the USA: a cross-sectional analysis of data from the California Lupus Epidemi-ology Study. *Lancet Rheumatol* 2024;**6**:e105−14.
15. Tian JR, Zhang DY, Yao X, Huang YQ, Lu QJ. Global epidemiology of systemic lupus erythematosus: a comprehensive systematic analysis and modelling study. *Ann Rheum Dis* 2023;**82**:351−6.
16. Gianfrancesco MA, Dall'Era M, Murphy LB, Helmick CG, Li J, Rush S, et al. Mortality among minority populations with systemic lupus ery-thematosus, including Asian and Hispanic/Latino persons - California, 2007−2017. *MMWR Morb Mortal Wkly Rep* 2021;**70**:236−9.
17. Fanouriakis A, Kostopoulou M, Alunno A, Aringer M, Bajema I, Boletis JN, et al. 2019 update of the EULAR recommendations for the management of systemic lupus erythematosus. *Ann Rheum Dis* 2019;**78**:736−45.
18. Anders HJ, Saxena R, Zhao MH, Parodis I, Salmon JE, Mohan C. Lupus nephritis. *Nat Rev Dis Primers* 2020;**6**:7.
19. Atisha-Fregoso Y, Toz B, Diamond B. Meant to B: B cells as a ther-apeutic target in systemic lupus erythematosus. *J Clin Invest* 2021;**131**:e149095.
20. Barnas JL, Looney RJ, Anolik JH. B cell targeted therapies in auto-immune disease. *Curr Opin Immunol* 2019;**61**:92−9.
21. Jordan N, D'Cruz DP. Belimumab for the treatment of systemic lupus erythematosus. *Expert Rev Clin Immunol* 2015;**11**:195−204.
22. Merrill J, Buyon J, Furie R, Latinis K, Gordon C, Hsieh HJ, et al. Assessment of flares in lupus patients enrolled in a phase II/III study of rituximab (EXPLORER). *Lupus* 2011;**20**:709−16.
23. Sanz I, Lee FE. B cells as therapeutic targets in SLE. *Nat Rev Rheumatol* 2010;**6**:326−37.
24. Rovin BH, Furie R, Latinis K, Looney RJ, Fervenza FC, Sanchez-Guerrero J, et al. Efficacy and safety of rituximab in patients with active proliferative lupus nephritis: the lupus nephritis assessment with rituximab study. *Arthritis Rheum* 2012;**64**:1215−26.
25. Ahuja A, Teichmann LL, Wang HW, Dunn R, Kehry MR, Shlomchik MJ. An acquired defect in IgG-dependent phagocytosis explains the impairment in antibody-mediated cellular depletion in lupus. *J Immunol* 2011;**187**:3888−94.
26. Robinson JI, Md Yusof MY, Davies V, Wild D, Morgan M, Taylor JC, et al. Comprehensive genetic and functional analyses of Fc gamma receptors influence on response to rituximab therapy for autoimmu-nity. *EBioMedicine* 2022;**86**:104343.
27. Marinov AD, Wang HW, Bastacky SI, van Puijenbroek E, Schindler T, Speziale D, et al. The type II anti-CD20 antibody Obinutuzumab (GA101) is more effective than rituximab at depleting b cells and

treating disease in a murine lupus model. *Arthritis Rheumatol* 2021;**73**:826−36.

28. Gallagher S, Yusuf I, McCaughtry TM, Turman S, Sun H, Kolbeck R, et al. MEDI-551 treatment effectively depletes b cells and reduces serum titers of autoantibodies in mice transgenic for *Sle1* and human CD19. *Arthritis Rheumatol* 2016;**68**:965−76.

29. Merrill JT, Wallace DJ, Wax S, Kao A, Fraser PA, Chang P, et al. Efficacy and safety of atacicept in patients with systemic lupus erythematosus: results of a twenty-four-week, multicenter, randomized, double-blind, placebo-controlled, parallel-Arm, phase IIb study. *Arthritis Rheumatol* 2018;**70**:266−76.

30. Kansal R, Richardson N, Neeli I, Khawaja S, Chamberlain D, Ghani M, et al. Sustained B cell depletion by CD19-targeted CAR T cells is a highly effective treatment for murine lupus. *Sci Transl Med* 2019;**11**:eaav1648.

31. Jin XX, Xu Q, Pu CF, Zhu KX, Lu C, Jiang Y, et al. Therapeutic efficacy of anti-CD19 CAR-T cells in a mouse model of systemic lupus erythematosus. *Cell Mol Immunol* 2021;**18**:1896−903.

32. Mougiakakos D, Krönke G, Völkl S, Kretschmann S, Aigner M, Kharboutli S, et al. CD19-targeted CAR T cells in refractory systemic lupus erythematosus. *N Engl J Med* 2021;**385**:567−9.

33. Mackensen A, Müller F, Mougiakakos D, Böltz S, Wilhelm A, Aigner M, et al. Anti-CD19 CAR T cell therapy for refractory systemic lupus erythematosus. *Nat Med* 2022;**28**:2124−32.

34. Chau CH, Steeg PS, Figg WD. Antibody−drug conjugates for cancer. *Lancet* 2019;**394**:793−804.

35. Wang L, Zhu L, Zheng Z, Meng L, Liu H, Wang K, et al. Mevalonate pathway orchestrates insulin signaling *via* RAB14 geranylgeranylation-mediated phosphorylation of AKT to regulate hepatic glucose metabolism. *Metabolism* 2022;**128**:155120.

36. Wang L, Zheng ZG, Zhu LJ, Meng LC, Liu HL, Wang KK, et al. Geranylgeranyl pyrophosphate depletion by statins compromises skeletal muscle insulin sensitivity. *J Cachexia Sarcopenia Muscle* 2022;**13**:2697−711.

37. Zhang XQ, Wang H, Ma ZG, Wu BJ. Effects of pharmaceutical PEGylation on drug metabolism and its clinical concerns. *Expert Opin Drug Metab Toxicol* 2014;**10**:1691−702.

38. Lambert JM, Berkenblit A. Antibody−drug conjugates for cancer treatment. *Annu Rev Med* 2018;**69**:191−207.

39. Marques-Ramos A, Cervantes R. Expression of mTOR in normal and pathological conditions. *Mol Cancer* 2023;**22**:112.

40. Fasano S, Milone A, Nicoletti GF, Isenberg DA, Ciccia F. Precision medicine in systemic lupus erythematosus. *Nat Rev Rheumatol* 2023;**19**:331−42.

41. Davis LS, Reimold AM. Research and therapeutics-traditional and emerging therapies in systemic lupus erythematosus. *Rheumatol* 2017;**56**:i100−13.

42. Dumontet C, Reichert JM, Senter PD, Lambert JM, Beck A. Antibody-drug conjugates come of age in oncology. *Nat Rev Drug Discov* 2023;**22**:641−61.

43. Tarantino P, Ricciuti B, Pradhan SM, Tolaney SM. Optimizing the safety of antibody−drug conjugates for patients with solid tumours. *Nat Rev Clin Oncol* 2023;**20**:558−76.

44. He JX, Duan Q, Ran CY, Fu T, Liu Y, Tan WH. Recent progress of aptamer−drug conjugates in cancer therapy. *Acta Pharm Sin B* 2023;**13**:1358−70.

45. He J, Peng T, Peng Y, Ai L, Deng Z, Wang XQ, et al. Molecularly engineering triptolide with aptamers for high specificity and cytotoxicity for triple-negative breast cancer. *J Am Chem Soc* 2020;**142**:2699−703.

46. Fu C, Yu LF, Miao YX, Liu XL, Yu ZJ, Wei MJ. Peptide-drug conjugates (PDCs): a novel trend of research and development on targeted therapy, hype or hope?. *Acta Pharm Sin B* 2023;**13**:498−516.

47. Ostendorf L, Burns M, Durek P, Heinz GA, Heinrich F, Garantziotis P, et al. Targeting CD38 with daratumumab in refractory systemic lupus erythematosus. *N Engl J Med* 2020;**383**:1149−55.